JACS
JOURNAL OF THE AMERICAN CHEMICAL SOCIETY
Article
pubs.acs.org/JACS

Synthesis of Co^{II}–NO^- Complexes and Their Reactivity as a Source of Nitroxyl

Melody R. Walter,[†] Stephen P. Dzul,[‡] Andria V. Rodrigues,[‡] Timothy L. Stemmler,[‡] Joshua Telser,[§] Jeanet Conradie,[∥] Abhik Ghosh,[⊥] and Todd C. Harrop*[,†]

[†]Department of Chemistry and Center for Metalloenzyme Studies, The University of Georgia, 140 Cedar Street, Athens, Georgia 30602, United States

[‡]Departments of Pharmaceutical Sciences, Biochemistry, and Molecular Biology, Wayne State University, Detroit, Michigan 48201, United States

[§]Department of Biological, Chemical, and Physical Sciences, Roosevelt University, 430 South Michigan Avenue, Chicago, Illinois 60605, United States

[∥]Department of Chemistry, University of the Free State, 9300 Bloemfontein, Republic of South Africa

[⊥]Department of Chemistry and Center for Theoretical and Computational Chemistry, University of Tromsø, N-9037 Tromsø, Norway

Supporting Information

ABSTRACT: Metal-nitroxyl (M–HNO/M–NO^-) coordination units are found in denitrification enzymes of the global nitrogen cycle, and free HNO exhibits pharmacological properties related to cardiovascular physiology that are distinct from nitric oxide (NO). To elucidate the properties that control the binding and release of coordinated nitroxyl or its anion at these biological metal sites, we synthesized {CoNO}^{8} (**1**, **2**) and {CoNO}^{9} (**3**, **4**) complexes that contain diimine–dipyrrolide supporting ligands. Experimental (NMR, IR, MS, EPR, XAS, XRD) and computational data (DFT) support an oxidation state assignment for **3** and **4** of high spin Co^{II} (S_{Co} = 3/2) coordinated to $^3NO^-$ (S_{NO} = 1) for S_{tot} = 1/2. As suggested by DFT, upon protonation, a spin transition occurs to generate a putative low spin Co^{II}–^{1}HNO (S_{Co} = S_{tot} = 1/2); the Co–NO bond is ∼0.2 Å longer, more labile, and facilitates the release of HNO. This property was confirmed experimentally through the detection and quantification of N_2O (∼70% yield), a byproduct of the established HNO self-reaction (2HNO → N_2O + H_2O). Additionally, **3** and **4** function as HNO donors in aqueous media at pH 7.4 and react with known HNO targets, such as a water-soluble Mn^{III}-porphyrin ($[Mn^{III}(TPPS)]^{3-}$; TPPS = *meso*-tetrakis(4-sulfonatophenyl)porphyrinate) and ferric myoglobin (metMb) to quantitatively yield $[Mn(TPPS)(NO)]^{4-}$ and MbNO, respectively.

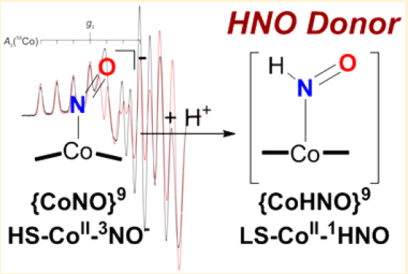

INTRODUCTION

Metal-nitroxyl (HNO/NO^-, pK_a = 11.6[1]) complexes represent critical intermediates in the global nitrogen cycle and inhibited states of metalloenzymes that lead to a variety of disorders.[2−4] For example, Fe–HNO intermediates are generated in the reduction of nitric oxide (NO) to nitrous oxide (N_2O), a detoxification path in fungal[5−7] and bacterial reductases (NORs).[8] Cytochrome *c* nitrite reductase (C*c*NiR),[9,10] responsible for the six-electron reduction of NO_2^- to NH_3, goes through two Fe–nitroxyl intermediates, designated as {FeNO}^{8} in the notation by Enemark and Feltham.[11] The extent of the Fe–NO_x π-backbonding in C*c*NiR prevents the release of any NH_xO_y intermediates during catalysis.[10] HNO-bound myoglobin (MbHNO) has also been well documented, likely due to its uncommon stability.[12,13] In addition to Fe proteins, cobalamins (Cbl), which serve as cofactors for vitamin B_{12}-dependent enzymes such as methionine synthase and methylmalonyl CoA-mutase,[14] are known to react with NO and HNO to form the corresponding {CoNO}^{8} complex NOCbl.[15−19] Indeed, inhibition and/or deficiency of Cbl, which results from interactions with NO, among other reasons, has been shown to lead to megaloblastic anemia and neurological disorders.[20,21]

In addition to representing intermediates in NO_x reduction, the pharmacological roles of HNO are rapidly emerging.[22−24] Despite its structural similarity, nitroxyl has therapeutic advantages distinct from NO,[25−27] probably due to its preference for thiols and Fe^{III}-hemes. For example, HNO increases heart muscle strength (positive cardiac inotrope; increases myocardial contractility) and plasma levels of calcitonin gene-related peptide (CGRP), whose cardiovascular effects include vasodilation.[26,27] As a result, nitroxyl has been looked to as a promising cardiovascular therapeutic. While the endogenous formation of HNO has yet to be firmly established, possible candidates include NO synthase (in the absence of its

Received: June 8, 2016
Published: August 26, 2016

DOI: 10.1021/jacs.6b05896
J. Am. Chem. Soc. 2016, 138, 12459−12471

cofactor),[28] thiol-containing species such as H_2S[29−31] or $SSNO^-$,[32] and antioxidants such as tyrosine and ascorbate.[33] Unfortunately, the rapid self-reaction ($k = 10^6$ M^{-1} s^{-1})[34] of HNO to N_2O and H_2O makes its detection challenging. Moreover, the instability of HNO necessitates the use of donor molecules.[35−37]

Several classes of HNO donors, both organic and inorganic, have been employed in research and even clinically. For example, Angeli's Salt ($Na_2N_2O_3$), which generates HNO and NO_2^- at physiological pH, is the most studied and utilized donor.[23,35,38] Cyanamide ($H_2N-C\equiv N$) is a drug that is used as an antialcoholism agent;[39,40] it is oxidatively bioactivated by catalase and releases HNO and CN^- as a byproduct. The mechanism of action is the inhibition of aldehyde dehydrogenase, an enzyme that is vital to metabolism of ethanol, resulting in elevated blood acetaldehyde levels. Although a number of such donors have been found effective, each is condition-dependent and has limitations that hinder its widespread utility, including concomitant release of undesirable byproducts (e.g., NO_2^-, CN^-), short half-lives, or ineffective release of HNO under physiological conditions.[23,26] Thus, there is a clear need for more effective HNO delivery agents.[26,35]

Given that metal sites appear to be both biological HNO targets and potential HNO sources, our lab has initiated a program aimed at elucidating the structural, electronic, and reactive properties of metal-coordinated nitroxyls, formally $\{MNO\}^8$, through the synthesis of coordination complexes that resemble biological active sites.[41−43] The objectives herein are two-fold: (i) to assess the ability of these systems to release HNO under physiological conditions; and (ii) to provide insight into the fundamental M−NO bonding properties in denitrifying enzymes that convert NO_x into reduced and bioavailable nitrogen compounds. We have previously communicated the five-coordinate (5C) $\{CoNO\}^8$ complex, $[Co(LN_4^{PhCl})(NO)]$ (LN_4^{PhCl} = dianion of (N^1E,N^2E)-N^1,N^2-bis((1H-pyrrol-2-yl)methylene)-4,5-dichlorobenzene-1,2-diamine, see Scheme 1), that exhibits H^+-induced release of

Scheme 1. Synthesis and Interconversion of $\{CoNO\}^8$ and $\{CoNO\}^9$ Complexes[a]

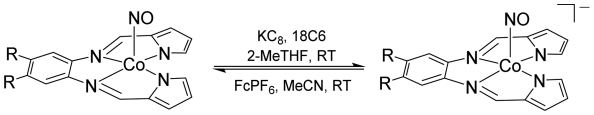

$\{CoNO\}^8$ (**1**, **2**)
$[Co(LN_4^{Ph})(NO)]$ (**1**)
$[Co(LN_4^{PhCl})(NO)]$ (**2**)

$\{CoNO\}^9$ (**3**, **4**)
$[K(18C6)][Co(LN_4^{Ph})(NO)]$ (**3**)
$[K(18C6)][Co(LN_4^{PhCl})(NO)]$ (**4**)

[a]R = H for **1**, **3**; R = Cl for **2**, **4**.

nitroxyl in organic solvents.[43] To realize HNO-release in water, we have synthesized and characterized the one-electron reduced $\{CoNO\}^9$ complexes in the present account (Scheme 1). While numerous $\{CoNO\}^8$ complexes exist,[41,43−54] few[53,55−58] describe NO release prior to our work. Furthermore, the $\{CoNO\}^9$ state is rare, with the exception of a few isolated tetrahedral complexes containing ligated carbonyls,[59,60] tris-pyrazolyl borates,[61,62] tris(2-diphenylphosphinoethyl)amines,[63,64] and one complex bearing an *N*-confused porphyrin.[65] However, the reaction chemistry of $\{CoNO\}^{8/9}$ systems is underexplored. Herein we report the synthesis and properties of 5C $\{CoNO\}^9$ complexes via a combined experimental and theoretical approach. Our results point to a high spin (HS) $Co^{II}-{}^3NO^-$ assignment for $\{CoNO\}^9$, which changes to low spin (LS) $Co^{II}-{}^1HNO$ upon protonation of the NO ligand. Most notably, the reported $\{CoNO\}^9$ complexes demonstrate the release of nitroxyl to Mn^{III}−P complexes (P = porphyrin) and Fe^{III}-myoglobin (metMb) in water at pH 7.4.

RESULTS AND DISCUSSION

Rationale. Addressing the structure and reaction chemistry of well-defined, first-row metal-coordinated nitroxyls has been challenging. Indeed, previous work by us[41,42] and others[2] (vide infra) demonstrate that $\{FeNO\}^8$ complexes, formally LS−$Fe^{II}-NO^-$, can be synthesized and generate coordinated HNO. However, these systems are very reactive, as they are highly susceptible to disproportionation, and thus necessitate the use of in situ low-temperature measurements. Employing Co to access coordinated nitroxyl or its anion provides a more controllable platform to explore and characterize biologically relevant M−HNO structure and bonding, as $\{CoNO\}^8$ complexes are stable and inert entities arising from the LS−$Co^{III}-NO^-$ assignment. Entry into the relatively unknown $\{CoNO\}^9$ state will afford reactive complexes that are more capable of HNO release, but less reactive than analogous Fe systems, due to $Co^{III}-NO^- \rightarrow Co^{II}-NO^-$ reduction. As such, Co-NO platforms can shed fundamental insights into the effects of metal oxidation state on coordinated NO^- reactivity. In addition, CoNO complexes will provide answers regarding the efficacy of Cbl as an HNO scavenger[17−19] and the potential use of NOCbl as an HNO donor.[66] The electronic structure of $\{CoNO\}^9$ is also more readily assessed by EPR hyperfine interactions with the $I = 7/2$ ^{59}Co nucleus (100% abundance), a feature that is lacking in reactive and diamagnetic $\{FeNO\}^8$ systems. Indeed, research and development of low molecular weight Co complexes has provided the community with materials utilized for H_2 evolution (alternative energy),[67−72] nitrite reduction (wastewater remediation and synthesis of reduced nitrogen compounds),[52] and the reductive activation of other small molecules of biological/environmental/industrial interest such as N_2[73,74] and CO_2,[75] reactions typically carried out in nature by Fe active sites.

Synthesis and Spectroscopy of $\{CoNO\}^8$ Complexes. The $\{CoNO\}^8$ complexes $[Co(LN_4^{Ph})(NO)]$ (**1**) (LN_4^{Ph} = dianion of (N^1E,N^2E)-N^1,N^2-bis((1H-pyrrol-2-yl)methylene)-benzene-1,2-diamine) and $[Co(LN_4^{PhCl})(NO)]$ (**2**)[43] were synthesized in ∼80% yield by direct purge of NO(g) into MeCN solutions of the parent $Co^{II}-LN_4^R$ complexes. Peripheral variations on the phenylene-diimine unit were made to explore ligand inductive effects on the redox properties of the Co-nitrosyls. Their structure and purity were confirmed by a variety of spectroscopic techniques as well as elemental analysis and X-ray crystallography (vide infra). For example, the FTIR spectrum of **1** displayed a strong double-humped ν_{NO} band at 1667 and 1656 cm^{-1} (KBr) that shifted to 1641 cm^{-1} ($\Delta\nu_{NO}$: 26 cm^{-1}) and 1628 cm^{-1} ($\Delta\nu_{NO}$: 28 cm^{-1}) upon isotopic substitution with ^{15}NO(g) (see Figure S1 in the Supporting Information (SI)). The morphology of the ν_{NO} peak in **1** is attributed to a disordered nitrosyl, which is seen in the X-ray structure (Figure S4). The ^{15}N NMR of the ^{15}N-labeled complex (**1**-^{15}**NO**) in THF-d_8 exhibited one ^{15}N peak at 675 ppm (vs CH_3NO_2) and is consistent with a bent metal-nitrosyl, i.e., ∠Co−N−O of ∼125° (Figure S3).[76] As noted with other 5C square-pyramidal $\{CoNO\}^8$ complexes,[41,43−54] these properties suggest a general assignment of LS-Co^{III} (S_{Co} =

DOI: 10.1021/jacs.6b05896
J. Am. Chem. Soc. 2016, 138, 12459−12471

0) coordinated to singlet nitroxyl anion $^{1}NO^{-}$ ($S_{NO} = 0$) for an overall diamagnetic ground state. We note that the resonance structure LS−Co^{III}−$^{1}NO^{-}$ ↔ LS−Co^{II}−$NO^{\bullet}$ has also been evoked for the {CoNO}^{8} unit in NOCbl.[15]

{CoNO}^{8} Structural Properties. Analogous to **2** and other 5C {CoNO}^{8} complexes,[41,43−54] the structure of **1** indicates a square-pyramidal (τ = 0.013[77]) Co with a mostly planar N_4 ligand and an axially bound NO (Figure 1, Tables S1−S2). Co

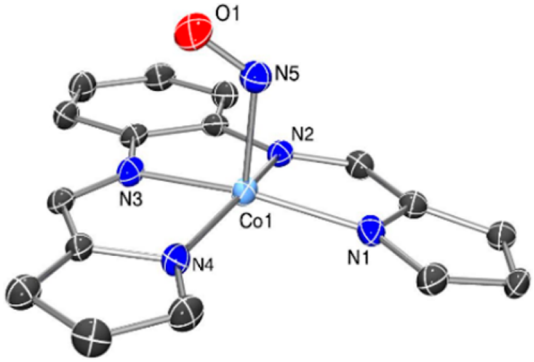

Figure 1. X-ray structure of one of two independent molecules in the lattice of [Co(LN_4^{Ph})(NO)] (**1**) at 50% thermal probability for all non-hydrogen atoms. Hydrogen atoms are omitted for clarity.

is displaced by 0.242 Å out of the plane of the N_4 ligand with Co−N(O) (1.804 Å) and N−O (1.162 Å) bond lengths typical for this class of metal-nitrosyls. For comparison, the N−O bond distance in **1** and **2** (1.162, 1.172 Å, respectively) is in between those of $NO^{\bullet}$ (1.15 Å) and HNO (1.21 Å) and suggests some degree of delocalization in the Co−N−O bond.[44] It appears that the range of N−O bond lengths observed in the majority of 5C pyramidal {CoNO}^{8} (1.15−1.20 Å) advocates for an NO^{-} oxidation state, which is reflected in the bent Co−N−O angle, 124.9°. The bent Co−N−O observed in the structure of **1** and other {CoNO}^{8} complexes is consistent with sp^2 hybridization of the nitrosyl nitrogen, which is also in-line with the solution-state ^{15}N NMR spectrum (vide supra).

Electrochemical Properties. The cyclic voltammogram (CV) of **1** was measured in MeCN and is reported versus the ferrocene/ferrocenium (Fc/Fc^{+}) couple. The CV of **1** displays a reversible {CoNO}^{8}/{CoNO}^{9} couple at −1.39 V (Figures S5−S7; $E_{1/2}$ = −0.99 V vs NHE). Other irreversible peaks observed in the CV are attributed to ligand-based redox events (Figure S5). Comparisons can be made with related Co−NO complexes and with metal-nitrosyls that also contain dianionic planar ligands. For example, **1** exhibits an $E_{1/2}$ value that is shifted by −0.11 V from **2**, which contains a more electron-deficient N_4 ligand. This result is consistent with the shift in the {FeNO}^{7}/{FeNO}^{8} couple observed in the Fe analogues reported previously by our lab.[42] Additionally, the {CoNO}^{8}/{CoNO}^{9} couple is readily modulated by changes beyond the ligand periphery. Indeed, attachment of $W(CO)_4$ to the coordinated thiolates in a Co(N_2S_2)(NO) complex results in a dramatic +0.49 V shift in $E_{1/2}$.[51] Overall, the reversible {CoNO}$^{8/9}$ couple of **1**, **2**, and other {CoNO}^{8} complexes[41,43,51,52] highlights the potential for accessing one-electron reduced {CoNO}^{9} complexes.

{CoNO}^{9} Synthesis and Properties. {CoNO}^{9} complexes were synthesized by adding stoichiometric KC_8 to a 2-MeTHF solution of **1** or **2** containing 18-crown-6 ether (18C6) (Scheme 1). Accordingly, the {CoNO}^{9} complexes [K(18C6)][Co(LN_4^{Ph})(NO)] (**3**) and [K(18C6)][Co(LN_4^{PhCl})(NO)] (**4**) were obtained in analytically pure form in 70 and 82% yields, respectively. The isolated brown {CoNO}^{9} complexes could also be converted back to the corresponding {CoNO}^{8} complexes **1** and **2** by addition of oxidants such as Fc^{+} (Scheme 1). Similarly, air oxidation leads primarily to {CoNO}^{8} with minor formation of Co−nitrite/nitrate complexes based on IR.

Spectroscopic analysis confirmed the {CoNO}^{9} assignment for **3** and **4**. The FTIR spectrum of **3** exhibited a ν_{NO} band at 1609 cm^{-1} that shifted to ∼1580 cm^{-1} in **3**-^{15}**NO** ($\Delta\nu_{NO}$ = 29 cm^{-1} from **3**; Figures S8−S9), whereas **4** exhibited ν_{NO} at 1617 cm^{-1}. Values of ν_{NO} for **3** and **4** resemble those reported for other {CoNO}^{9} complexes.[52,59−65] The ν_{NO} of **4**-^{15}**NO** overlaps significantly with ligand C═N stretches, making a definitive assignment difficult (Figure S10). Similar complications in identifying ν_{NO} bands have also been observed in an {FeNO}^{8} porphyrin complex due to overlapping ligand vibrations.[78] Regardless, the ν_{NO} peaks of **3** and **4** are ∼50 cm^{-1} red-shifted from the {CoNO}^{8} analogs, a shift which is consistent with a Co-centered reduction. In comparison, reduction of coordinated NO generally results in a dramatic ν_{NO} red-shift (∼100−200 cm^{-1}), as observed in the reduction of {FeNO}^{7} to {FeNO}^{8}.[2,4,79,80] Moreover, ligand-based redox events to generate pyrrolide radicals[81] can be eliminated based on EPR data (vide infra). High resolution mass spectrometry (HRMS) experiments provide additional evidence for the formation of **3** and **4**. For example, the molecular ion peak $[M]^{-}$ for **3** is observed at *m/z*: 349.037 (calcd. *m/z*: 349.037) with the appropriate isotopic distribution (Figure S11). HRMS on the ^{15}N isotopologue **3**-^{15}**NO** (calcd. *m/z*: 350.034; obsvd. *m/z*: 350.035) further supports the predicted formulation (Figure S12). HRMS also confirms formation of **4** and **4**-^{15}**NO** (Figures S13−S14).

EPR of {CoNO}^{9} Complexes. X-band (9.60 GHz) measurements of **3** and **4** reveal an asymmetric coordination environment with significant nuclear hyperfine coupling (hfc) from the ^{59}Co nucleus (I = 7/2) whereas the ^{14}N splitting is minimal (Figure 2; Figure S15). The large ^{59}Co hfc differs from EPR of Co^{II}−O_2 complexes[82,83] and from typical LS-Co^{II}, where the unpaired electron (upe) is in the d_{z^2} orbital, leading to $g_{\perp} > g_{\parallel} \approx 2.0$, large $A_{\parallel}(^{59}Co)$, and small $A_{\perp}(^{59}Co)$.[84−86] For example, the spin Hamiltonian parameters of [Co^{II}(OEP)L] complexes (where OEP = octaethylporphyrin; L is a wide range of N-donors, e.g., py, Im), in which the upe resides in the d_{z^2} orbital, were reported with $g_{\parallel}$ = 2.03 ± 0.01 and $A_{\parallel}(^{59}Co)$ = 225−240 MHz (∼80−85 G) and with $g_{\perp}$ = 2.315 ± 0.010, where $A_{\perp}(^{59}Co)$ is small (<10 MHz, 3 G) and unresolved.[84] Contrastingly, **3** and **4** exhibit $g_{\parallel} > g_{\perp}$ ($g_{\parallel}$ = 2.270, $g_{\perp}$ = 2.070, 2.085; $g_{\parallel}$ = 2.278(2); $g_{\perp}$ = 2.078(2), respectively) and both $A_{\perp,\parallel}$ values are large (∼200 MHz and ∼350 MHz, respectively) (Figure 2). This result indicates the upe being predominantly in the $d_{x^2-y^2}$ orbital,[87] resembling what is commonly seen in square-planar/pyramidal Cu^{II} complexes.[88,89] Further support of a $d_{x^2-y^2}$ upe is shown in the proposed frontier MOs (vide infra) and in comparison to other M−NO systems. In a cyclam-ligated {FeNO}^{6} complex, calculations of frontier MOs using spin-restricted B3LYP suggest the NO-π^* orbital is lower in energy than the nearby $d_{x^2-y^2}$ orbital.[90] In contrast to the {FeNO}^{6} case, it is likely that the NO-π^* orbital in **3** and **4** is higher in energy than $d_{x^2-y^2}$ due to stronger π-bonding in Co−N versus Fe−N. Due to the high covalency of the Co−N(O) bond, the effect of the equatorial N-ligands can be detected by inspection of EPR linewidths.[91] The X-band EPR of the

DOI: 10.1021/jacs.6b05896
J. Am. Chem. Soc. 2016, 138, 12459−12471

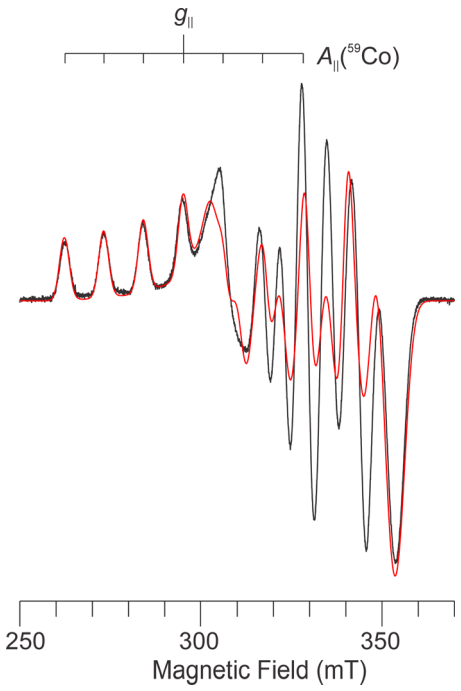

Figure 2. X-band EPR spectrum of **3** in 2-MeTHF at 10 K (black) with simulation (red). Spectrometer settings: microwave frequency, 9.582 GHz; microwave power, 1.0 mW; modulation frequency, 100 kHz; modulation amplitude, 6.48 G. Simulation parameters: $S_{tot} = 1/2$, g = [2.070, 2.085, 2.270], collinear $A(^{59}Co)$ = [200, 180, 355] MHz (so that $A_{\perp}(^{59}Co)$ = 190 MHz), single crystal Gaussian line widths, $W_{\perp}$ = 80 MHz, $W_{||}$ = 40 MHz (half-width at half-maximum).

isotopologues **3**-^{15}**NO** and **4**-^{15}**NO** (^{15}N, $I = 1/2$) exhibits no significant effect from labeling on the ^{59}Co hfc, although there is an increase in the EPR linewidths, indicative of unresolved ^{14,15}N hfc. This is further indication that the majority of the spin-density is on Co.[62]

The X-band EPR is modeled as very slightly rhombic; as such, higher frequency EPR (Q-band; 35 GHz) spectra were recorded in order to obtain better dispersion of the g-values (which are field-dependent). However, the field-independent hfc is more readily determined from lower frequencies (X-band or even lower (S- or L-band)[92] EPR). This multifrequency approach has been pervasive for Cu^{II} complexes,[93] but only recently applied to LS-Co^{II} species.[94] The Q-band EPR corroborates the X-band measurement (Figure S16), and resolution of slight rhombic splitting is attainable with the higher frequency. The Q-band spectrum of **3** (200(10), 200(10), 345(5); W = 130 MHz) was simulated with similar $A(^{59}Co)$ values as in the X-band data (200(5), 200(5), 355, W_{xy} = 80 MHz), and the $g_{\perp}$ obtained from the X-band simulation ((2.070 + 2.085)/2 = 2.078(2)) is exactly the average of the resolved Q-band $g_{x,y}$ values (2.06(1), 2.10(1)) (Figure S16). It is important to note that, even at Q-band, {CoNO}^{9} complexes **3** and **4**, comprising the two different ligands LN_4^{Ph} and LN_4^{PhCl}, respectively, give identical EPR spectra, indicating a negligible effect of peripheral substitution on the Co center.

Overall, the multifrequency EPR studies demonstrate that both {CoNO}^{9} complexes, **3** and **4**, are Co-centered paramagnets, as opposed to nitroxyl radicals bound to essentially diamagnetic metals. As seen by EPR, **3** and **4** have essentially axial symmetry, as found, e.g., in porphyrin complexes, which is unsurprising given the roughly square-planar N_4 donor set from LN_4^R, but the frontier molecular orbitals are opposite: typical LS Co^{II}–L_{ax} porphyrins have the upe in a d_{z2} orbital, with d_{x2-y2} unoccupied, while the ground state in **3** and **4** has the upe in d_{x2-y2} with d_{z2} unoccupied. Computational studies (vide infra) probe the electronic structure of these {CoNO}^{9} systems quantitatively.

X-ray Absorption Spectroscopy (XAS) of {CoNO}$^{8/9}$ Complexes. The XAS data confirm the crystallographic results of **1** (Figures 3 and 4). XAS spectra are constructed of two components: the X-ray absorption near edge spectrum (XANES), which provides electronic and structural insight regarding metal oxidation state and metal–ligand coordination symmetry, and the extended X-ray absorption fine structure (EXAFS) region, which provides highly accurate metal–ligand bond length characterization (±0.02 Å), metal ligand coordination number (±0.5), and ligand atom identity (±row of the periodic table).[95] In the XANES of **1**, the lowest energy pre-edge peak occurs at 7710.1 eV, which corresponds to a symmetry-forbidden 1s → 3d transition. The relatively large

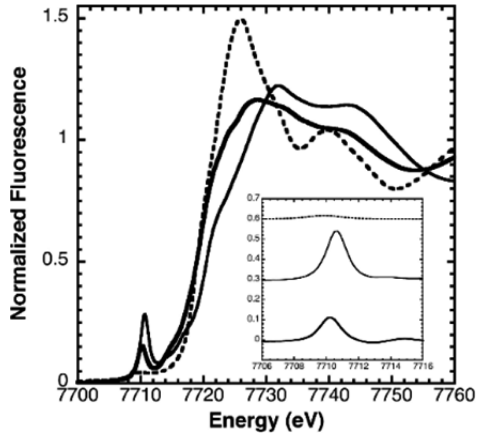

Figure 3. XANES for {CoNO}^{8} **1** (normal), {CoNO}^{9} **3** (bold), and $[Co^{II}(H_2O)_6](NO_3)_2$ (dotted). Inset: baseline subtracted expansion of 1s → 3d pre-edge features for **1**, **3**, and Co^{II} control, offset for clarity (coding same as XANES).

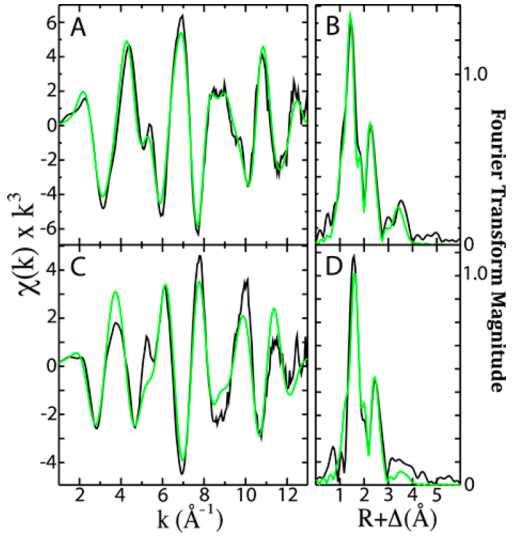

Figure 4. Raw (panels A, C) and Fourier transformed EXAFS (panels B, D) (black) of {CoNO}^{8} **1** (top) and {CoNO}^{9} **3** (bottom) with best fit simulation (green).

DOI: 10.1021/jacs.6b05896
J. Am. Chem. Soc. 2016, 138, 12459–12471

area under this transition (0.44 eV) is consistent with an increased distortion in bond symmetry that permits mixing of 3*d* and 4*p* orbitals in the formation of a LS 5C Co complex.[96] The first inflection point of the XANES is shifted to higher energy relative to the Co^{II} control, which is indicative of reduced electron density on the metal and more consistent with a Co^{III} oxidation state in **1**. Simulations of the extended X-ray absorption fine structure (EXAFS) region show an average bond length in the nearest neighbor environment for **1** of 1.88 Å, constructed of five O/N ligands (spectral resolution: 0.12 Å) (Figure 4). This value compares well with the distances determined from X-ray crystallography (avg: 1.89 Å, Table S2). The XAS of **2** is also comparable to **1**.[43]

The XAS of **3** shows distinct features that correspond to a Co-centered reduction when going from $\{CoNO\}^8$ to $\{CoNO\}^9$. The XANES region of the spectrum displays a 1s → 3d pre-edge feature at 7709.7 eV for **3** (shifted −0.4 eV from **1**), and the first inflection point of the edge feature aligns closely in energy to the Co^{II} model (Figure 3), suggesting a Co^{II} center in **3**, consistent with EPR. The 1s → 3d feature in this region has also been observed in a tetrahedral $\{CoNO\}^9$ complex[62] and other 5C/6C Co^{II} complexes.[96,97] The area under this transition is an indication of the symmetry about the Co center. In general, more centrosymmetric complexes exhibit weaker 1s → 3d transitions. Indeed, the area of the pre-edge feature of **3** (0.18 eV) is less than in **1** (0.44 eV), which suggests a more symmetric coordination environment in **3** versus **1** (Figure 3). A change in either coordination geometry (centrosymmetric, e.g., octahedral or square-planar) or spin-state could explain the weaker pre-edge intensity. However, EPR (vide supra) in combination with EXAFS (vide infra), eliminate a geometry change. For example, octahedral and planar Co^{II} complexes exhibit very weak 1s → 3d peaks with areas ranging from 0.050 to 0.061 eV.[98] As the EXAFS and computational (vide infra) results confirm, a 5C coordination sphere is retained in **3** and **4**. Thus, the symmetry difference between **1** and **3** is likely associated with a change in the Co−N−O bond angle from bent (~125°) in $\{CoNO\}^8$ (**1**, **2**) to less bent but still not linear (140−150°) in $\{CoNO\}^9$ (**3**, **4**).

A comparison of the EXAFS for **1** and **3** shows completely different wave patterns, suggesting significant changes in the metal−ligand metrical parameters between these two molecules. Simulations of the EXAFS region of **3** show an average bond length of 2.06 Å constructed of 4 ± 1 O/N ligands (Figure 4, Table S3). Based on the large Debye−Waller factor ($\sigma^2 = 4.14 \times 10^3$ Å^2) in the nearest neighbor fit for **3**, there is a higher level of metal−ligand bond disorder for this system, which explains the abnormally low apparent metal−ligand coordination number. Furthermore, based on the chemical reversibility of the **3**-to-**1** conversion, a 5C Co is still expected in **3**. This average distance compares well with distances determined from EXAFS analysis of other N-ligated Co^{II} complexes, such as Co-substituted ferric uptake regulatory protein[99] and Co^{II}-substituted alcohol dehydrogenase.[100] The EXAFS also indicates there is an increase in the Co-ligand distances between $\{CoNO\}^8$ **1** and $\{CoNO\}^9$ **3** of 0.18 Å, a shift which is again consistent with a metal-based reduction. Similar metric changes are also observed for **4** (see Table S3).

Theoretical Modeling. Density functional theory (DFT) calculations provide a satisfactory theoretical framework for understanding many of the properties of the $\{CoNO\}^9$ state outlined above.[101,102] The assumption of C_s symmetry allowed us to investigate at least two different states. All-electron occupation 1 ($\alpha\|\beta$: A′ 61‖60, A″ 45‖45) corresponds to a LS d^7 Co^{II} state with the eighth and ninth electrons (Enemark−Feltham count) added to a ligand (NO π^* or other) orbital (Figure S19).[103] Occupation 2 ($\alpha\|\beta$: A′ 60‖60, A′′ 46‖45) is described as a HS Co^{II}-NO^- state with a singly occupied d_{x2-y2} orbital (Figures 5 and 6). All functionals tested (BP86, OLYP, B3LYP) indicate occupation 2 as the ground state, in agreement with the EPR data, albeit by different margins of energy, relative to occupation 1 (Figure S19). Some of the key calculated properties of occupation 2 follow.

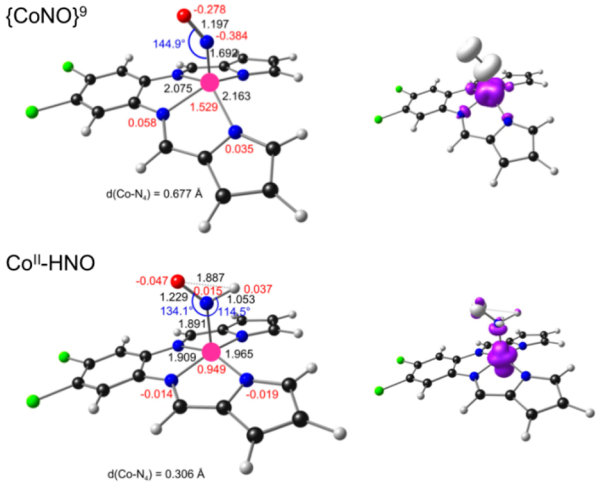

Figure 5. Selected OLYP/TZP results for the lowest-energy $\{CoNO\}^9$ (top) and Co^{II}-HNO (bottom) states: optimized structures on the left with distances (Å, black), angles (deg, blue), and Mulliken spin populations (red); spin density profiles on the right. Majority and minority spin densities are indicated in purple and ivory, respectively.

Single occupancy of the d_{x2-y2} orbital resulted in relatively long equatorial Co−N distances of about 2.1 Å, relative to occupation 1 and the $\{CoNO\}^8$ state (Co−N: 1.9 Å; see Figure S20), in agreement with the EXAFS results. This orbital occupancy is also responsible for a substantial displacement of the metal (~0.7 Å) above the N_4 plane of the ligand, a structural effect that remains to be observed experimentally. The Co−N(O) bond length is 1.692 Å, essentially unchanged from the $\{CoNO\}^8$ state. Another significant structural change is the less bent nature of Co−N−O (144.9°) in $\{CoNO\}^9$, which explains the intensity change of the 1s → 3d feature in the XAS.

The spin density profile for occupation 2 is characterized by a full unpaired electron in the d_{x2-y2} orbital, smaller amounts of positive spin density in the d_{xz} and d_{yz} orbitals, and a significant amount of negative spin density on the NO distributed in a cylindrically symmetric manner about the N−O axis (Figure 5). These spin populations are indicative of HS Co^{II}, ($S_{Co} = 3/2$) with a $(d_{xy})^2(d_{z2})^2(d_{xz})^1(d_{yz})^1(d_{x2-y2})^1$ configuration, antiferromagnetically coupled to an NO^- diradical ($S_{NO} = 1$). The reader may verify this orbital occupancy from a careful examination of the frontier MOs (Figure 6).

The spin density profiles obtained with the three functionals differ somewhat. As noted before, the hybrid functional B3LYP resulted in the largest spatial separation of α and β spin density, the classic pure functional BP86 resulted in the smallest such separation, and the comparatively newer OLYP functional separated the α and β spins to an intermediate degree. Despite the quantitative differences, the fact that all three functionals

DOI: 10.1021/jacs.6b05896
J. Am. Chem. Soc. 2016, 138, 12459−12471

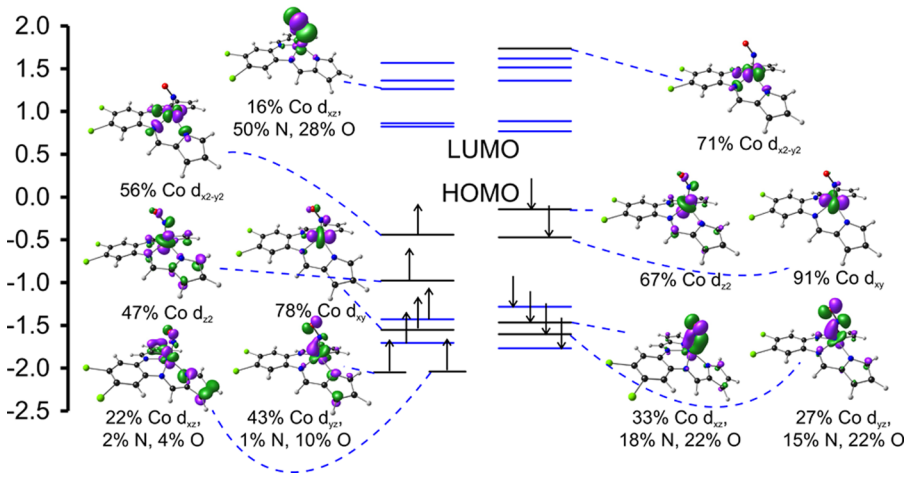

Figure 6. OLYP/TZP Kohn–Sham energy level diagram (vertical scale is in eV) for the frontier MOs of the $\{CoNO\}^9$ system. Energy levels shown as black lines have substantial Co *d* character; those shown as blue lines are mostly ligand-based.

indicate occupation 2 as the ground state may be viewed as powerful evidence in support of our electronic structural description.[104] As mentioned, this description is fully consistent with the conclusion from XAS and EPR.

DFT (OLYP) calculations on the Co–HNO complex indicate a low-spin d_{z2}^1 Co^{II} ground state axially coordinated to a closed shell HNO (Figure 5). The singly occupied molecular orbital (SOMO) represents a σ-antibonding interaction between the Co d_{z2} (43.4%) and NO p_z (17.7%). Such an electronic description is consistent with a longer Co–N(O) (1.891 Å) and N–O (1.229 Å), and shorter equatorial Co–N (avg: 1.937 Å), relative to the $\{CoNO\}^9$ state (Figures 5 and S21). The lengthening of Co–N(O) is important, as it primes the HNO for dissociation and further reactivity, and reflects the relatively weak π-acceptor ability of HNO (compared with NO) as well as the antibonding nature of the SOMO. The calculations did not reveal any other low-energy states for the Co–HNO complex; assumption of M_S = 3/2 led to a high spin Co^{II} ~ 0.5 eV above the ground state.

Nitroxyl-Relevant Reactivity in Water. *Reaction of {CoNO}^{9} Complexes with H$^+$ and Formation of HNO.* Given the fast self-reaction of nitroxyl[34] to form N_2O and water (vide supra), N_2O serves as an indirect marker for HNO, and its presence provides evidence of the formation and liberation of HNO from the reported CoNO complexes.[104] After addition of $HBF_4{\cdot}Et_2O$ to $\{CoNO\}^9$ (**3**) in H_2O (10:1), the reaction headspace revealed IR bands consistent with the P- and R-branches of N_2O at 2236 and 2208 cm^{-1} that shift to 2167 and 2145 cm^{-1} when using the ^{15}NO isotopologue (Figure 7).[8,105,106] Indeed, the yield of N_2O from **3** was 63 ± 3%, quantified using a calibration curve with N_2O produced from the HNO donor Piloty's Acid (Figure S22).[107] These results were consistent with the **4**/H^+ reaction. *Thus, {CoNO}^{9} complexes produce HNO in water.* Notably, no other gaseous ^{15}N-containing species were observed in the IR (Figure S23). Reaction of **3** with $HBF_4{\cdot}Et_2O$ (1:7) in THF, a solvent in which other products are readily identified, also produces N_2O. Additional species identified in the THF reaction were $\{CoNO\}^8$ **1**, as well as the corresponding tetrahedral dinitrosyl cobalt complex $[Co(LN_4^{Ph}H_2)(NO)_2]BF_4$ (**5**, a $\{Co(NO)_2\}^{10}$ complex; Figures S24–S25) via protonation of the pyrrolide-N-donors of LN_4^{2-}.[108] Contrastingly, $\{CoNO\}^8$ complexes (**1**, **2**) are not reactive, likely due to a lower HNO pK_a, and largely

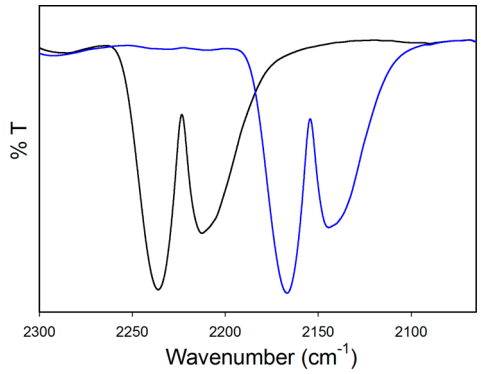

Figure 7. Headspace IR of the reaction of $HBF_4{\cdot}Et_2O$ with **3** (black) or **3**-^{15}**NO** (blue) (10:1) at *t* = 24 h. Conditions: DMSO/H_2O (1:9), RT. See Figure S23 for full spectrum.

H_2O-insoluble, precluding **1** or **2** from effectively releasing HNO in water.[109]

To this point (2016), few first-row metal–nitroxyl complexes demonstrating release of HNO have been reported. Tetrahedral dinitrosyl iron complexes (DNICs) bearing N-[110] and S-supporting[110,111] ligands exhibit HNO-transfer capability to Fe^{III}-heme proteins and Fe^{III}-porphyrins; however, no measurements have been done to track the possibility of free HNO. Lehnert synthesized a sterically protected $\{FeNO\}^8$ porphyrin, which forms an Fe–HNO complex revealed by UV–vis at RT. While this design prevented the disproportionation chemistry often seen in Fe-nitroxyls, HNO release was not observed.[112] Richter-Addo reported the in situ synthesis and characterization of an Fe-HNO porphyrin that reacts with Ph_3P, a well-known HNO trap,[113] to yield $Ph_3P{=}O$ and $Ph_3P{=}NH$.[114] However, the phosphine products were not quantified and other methods to test HNO release were not provided. Ultimately, this complex decomposes to the corresponding $\{FeNO\}^7$ and H_2 even at −20 °C. Additionally two $\{FeNO\}^8$ complexes have been crystallized, yet addition of acid to these Fe-nitroxyls leads to either the $\{FeNO\}^7$ and H_2[78,115] or no reaction.[116] Multinuclear Fe complexes[8] release N_2O through an NOR-like reaction (NOR: $2NO + 2e^- + 2H^+ \rightarrow N_2O + H_2O$) via coupling of closely spaced coordinated nitroxyl ligands. Importantly, mononuclear analogues of these Fe complexes *do not generate N_2O*, emphasizing the necessity of such

DOI: 10.1021/jacs.6b05896
J. Am. Chem. Soc. 2016, 138, 12459–12471

multinuclear entities. Most related to this work are two Co compounds that go through putative $\{CoNO\}^9$ intermediates to result in N_2O.[52,65] The $\{CoNO\}^9$ system with an *N*-confused porphyrin catalytically generates N_2O via a bimolecular NOR mechanism;[65] dimerization of free HNO to N_2O was excluded based on MS evidence of the hyponitrito-bridged Co-dimer. Notably, none of these studies collectively probe the HNO donor capacity of the Fe- or Co-nitroxyls, and only one demonstrated HNO transfer in water. These reports contrast with what we demonstrate here, viz., *no evidence of a dimer to promote N−N coupling via an NOR-like pathway* that would be independent of free HNO.

Reaction of $\{CoNO\}^{8/9}$ Complexes with a Nitroxyl Target (Mn^{III}-Porphyrin). Based on the high affinity and superior selectivity of HNO for Mn^{III}−P,[117] HNO donor reactions were investigated using water-soluble $[Mn^{III}(TPPS)]^{3-}$ (TPPS = *meso*-tetrakis(4-sulfonatophenyl)porphyrinate; λ_{max} = 467 nm) in phosphate-buffered saline (PBS; pH 7.4) at 298 K. Indeed, the reaction of **3** with $[Mn^{III}(TPPS)]^{3-}$ (5:1) afforded $[Mn(TPPS)(NO)]^{4-}$ (λ_{max} = 424 nm) in 6.5 h with a pseudo-first-order rate constant (k_{obs}) of 9.00 ± 3.96 × 10^{-5} s^{-1} (Figure 8). In contrast, no reaction was observed between

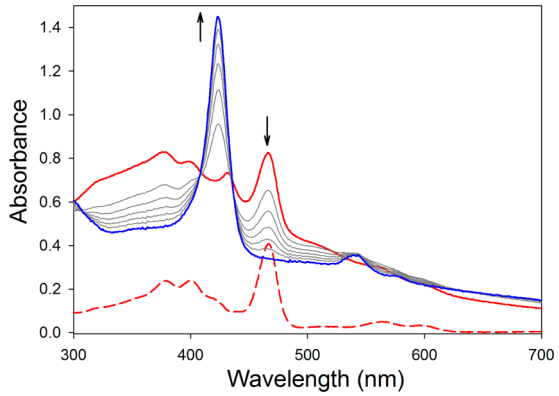

Figure 8. UV−vis spectral monitor of a 9.90 μM PBS solution (pH 7.4, 298 K) of $[Mn^{III}(TPPS)]^{3-}$ (red dash) and immediately after addition of **3** (red solid; 5 equiv). Final trace of $[Mn(TPPS)(NO)]^{4-}$ in blue (t = 6.5 h).

$\{CoNO\}^8$ **1** and $[Mn^{III}(TPPS)]^{3-}$ over a 24 h period under identical conditions (Figure S26). As demonstrated by Doctorovich,[117] the reaction between $[Mn^{III}(TPPS)]^{3-}$ and a large excess of Angeli's Salt occurs with $k_{obs} \sim 10^{-2}$ s^{-1} ($t_{1/2}$: 117 min) at pH 7. Additionally, they demonstrate that $E_{1/2}(Mn^{III}/Mn^{II})$ of Mn−P influences the reaction mechanism with HNO donors; viz., an Mn−P with $E_{1/2} > 0$ accelerates decomposition of the donor through a donor/Mn−P bonding interaction, whereas an Mn−P with $E_{1/2} < 0$ reacts directly with free HNO after donor decomposition.[118,119] This mechanistic distinction may be facilitated by electrostatics, given the negative charge of HNO donors such as Angeli's Salt and Piloty's Acid. Indeed, when Mn^{III}−P and the HNO donor directly interact, $t_{1/2}$ is on the order of seconds. In contrast, $t_{1/2}$ is on the order of minutes-to-hours when donor decomposition/release of free HNO is the rate-limiting step. The latter occurs when the Mn^{III}−P $E_{1/2}$ is negative. Taken together, the clean reaction of **3** with $[Mn^{III}(TPPS)]^{3-}$ ($E_{1/2}$ = −0.16 V vs NHE) to form the $\{MnNO\}^6$ complex over 6.5 h is consistent with production of free HNO from the $\{CoNO\}^9$ platform in **3**.

Given that one of the products of the $\{CoNO\}^9$ **3**/H^+ reaction in THF is the corresponding $\{Co(NO)_2\}^{10}$ complex **5**, we also probed the reaction between **5** and $[Mn^{III}(TPPS)]^{3-}$ (Figure S27). Based on UV−vis spectral monitoring, the reaction of **5** with $[Mn^{III}(TPPS)]^{3-}$ (2.5/1) goes to completion in 21 h. Thus, **5** is capable of reductively nitrosylating Mn^{III}−P and is an alternative HNO donor. This result draws parallels to thiolate-ligated $\{Fe(NO)_2\}^9$ DNICs that have been demonstrated to store and release NO equivalents in a proton-responsive manner.[120−122] However, it appears that $\{CoNO\}^9$ **3** reacts on a slightly faster time scale than its dinitrosyl analogue and is thus an unlikely HNO donor in the aforementioned reaction.

Reaction of $\{CoNO\}^{8/9}$ Complexes with a Biological Nitroxyl Target (metMb). Biological HNO targets were pursued to assess whether HNO/NO^- coordination occurs with known proteins under aqueous conditions. As such, the reaction of the Co-nitrosyls with equine skeletal metMb was investigated in PBS (pH 7.4) at 310 K. The addition of $\{CoNO\}^9$ **3** to metMb (5:1) afforded nitrosylated myoglobin (MbNO) over 1.5 h based on shifts in the Soret (409 nm → 420 nm) and Q-bands (503 nm, 637 nm → 545 nm, 582 nm; Figure 9). Using the ε values of metMb[123,124] and MbNO,[125]

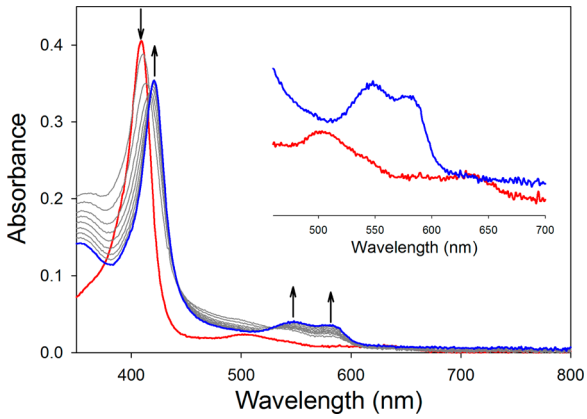

Figure 9. UV−vis spectrum of a 2.19 μM solution of equine skeletal muscle metMb before (red) and after 1.5 h (blue) reaction with **3** (5 equiv) at 310 K in PBS (pH 7.4; traces in gray represent 10 min intervals). Inset: expansion of the Q-band region for the initial and final spectrum.

formation of MbNO was found to be nearly quantitative[126] with k_{obs} = 4.88 ± 0.72 × 10^{-4} s^{-1}. Under similar conditions, the reaction of **4** with metMb was complete within 3.5 h (Figure S28). The $\{CoNO\}^9$/metMb reaction is slower than the immediate HNO/NO^- transfer that occurs with the analogous $\{FeNO\}^8$ system.[41] For reference, the reaction of Angeli's Salt with sperm whale metMb takes 15.5 min to go to completion,[127] and recently, a DNIC was shown to form MbNO in 10 min (both at 25 °C).[110] The slower HNO release of **3** is an advantageous kinetic control that we did not have with the Fe systems. In contrast, there was no reaction between **1** and metMb (Figure S29).

Mechanistically, there is no evidence of a reduced Fe^{II}-Mb intermediate (Soret = 435 nm[123]), although the timescale with which such an intermediate is formed and then nitrosylated could be more rapid than the timescale with which the reaction was monitored (<1 min). To eliminate the possibility that $\{CoNO\}^9$ reductively nitrosylates metMb by electron-transfer

DOI: 10.1021/jacs.6b05896
J. Am. Chem. Soc. 2016, 138, 12459−12471

followed by NO• release from {CoNO}^{8}, we studied the reaction of {CoNO}^{8} **1** with ferrous myoglobin (deoxyMb). Interestingly, complex **1** is capable of nitrosylating deoxyMb, to form MbNO (Figure S31). However, this reaction is complete soon after mixing the two compounds. If metMb reduction by {CoNO}^{9} occurred before nitrosylation, then the completion time would likely be faster than the observed 1.5 h. Therefore, these results, along with the Mn^{III}–P assay, suggest free HNO transfer from **3**. In contrast to its reaction with Mn^{III}–P, {Co(NO)$_2$}^{10} **5** is not capable of reductively nitrosylating metMb under identical conditions (24 h), likely a result of electrostatic repulsion between the positively charged metMb and the cationic dinitrosyl (Figure S32).

Proposed Reaction Pathway. Spectroscopic evidence (^{1}H NMR, IR, MS) of the **3**/H$^+$ reaction points to formation of free HNO via N_2O in addition to the presence of the Co-nitrosyl **1** and dinitrosyl **5** as major products. A smaller amount of [Co^{III}L]$^+$ and [Co^{I}L]$^-$ is also observed. Several paths that account for these compounds are depicted in Scheme 2. In the absence of an HNO target, three competing reactions occur. Reaction A produces free HNO, which self-reacts to form N_2O and H_2O. An alternate reaction (B) produces 1 equiv of {CoNO}^{8} **1** with concurrent evolution of 0.5 equiv of H_2. Reactions analogous to B have been reported[78,112,128] with an {FeNO}^{8} complex to form H_2 and the corresponding {FeNO}^{7}. Two of the reactions (B and C) account for the observation of dinitrosyl **5**. We have previously demonstrated that {CoNO}^{8} and H$^+$ are in equilibrium with {Co(NO)$_2$}^{10} and [Co^{III}L]$^+$ (Scheme 2, bottom).[43] The {CoNO}^{8}/H$^+$ equilibrium favors the reactant side under stoichiometric conditions. The other possibility (C) generates **5** with the concomitant production of a [Co^{I}L]$^-$ monoanion. These three competing reactions explain the observed product speciation, the diamagnetism, as well as the relative quantities based on NMR integration. Path A is favored with excess H$^+$ whereas B and C are favored under stoichiometric conditions. Assuming a pK_a of 11 for the Co-coordinated NO,[129] nearly all (99.8%) of the complex is Co-HNO at pH 7.4 and thus reaction A predominates under physiological conditions.

The first step toward free HNO is protonation of **3** to form **3-HNO**, which, as suggested by DFT, changes the Co from HS to LS, i.e., LS-Co^{II}-^{1}HNO (Scheme 3). Protonation leads to elongation of the Co–NO distance by 0.2 Å and labilizes this bond so that HNO can readily dissociate from the [Co^{II}L] platform. HNO can then either (i) form N_2O and/or (ii) react with an HNO target, e.g., [Mn^{III}(TPPS)]$^{3-}$ or metMb. Indeed, in the presence of an HNO target, the free HNO produced from **3** is captured (see Figures 7–9). As there is no spectral evidence for any intermediates in the {CoNO}^{9} reaction with metMb or Mn^{III}–P, and given the isosbestic behavior, it is likely that free HNO dissociates from Co and reacts with the M^{III}-P center directly.

Scheme 2. Interconversions of Co Nitrosyls upon Protonation in the Absence of an HNO Target[a]

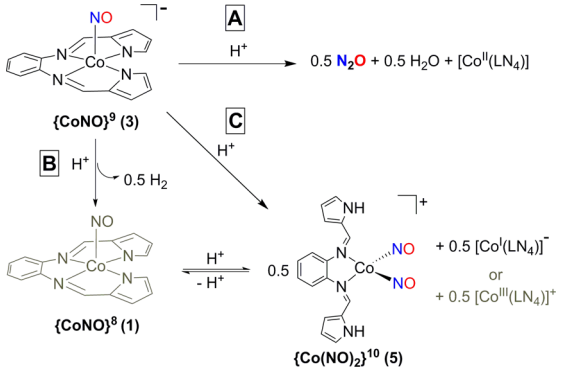

[a]Path A is favored with excess H$^+$.[108] Grey represents the {CoNO}^{8}/H$^+$ path.[43].

Scheme 3. Proposal of HNO-Release[a]

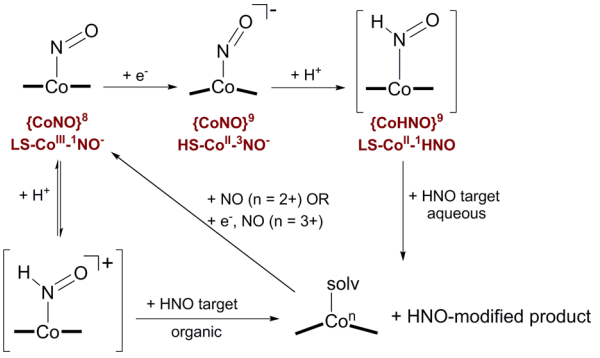

[a]Compounds in brackets represent intermediates not isolated or observed spectroscopically in the reaction.

CONCLUSIONS

A combined structural (XAS), spectroscopic (FTIR, EPR, MS) and theoretical (DFT) effort has shown that 5C {CoNO}^{9} species exhibit rare electronic structural properties that change upon the addition of H$^+$.[130,131] The isolated nitroxyl anion complexes (**3**, **4**) are assigned as HS–Co^{II} coordinated to ^{3}NO$^-$, while a putative LS–Co^{II}–^{1}HNO intermediate exists after H$^+$ addition. These protonated {CoNO}^{9} complexes liberate free HNO in water, as demonstrated by the detection and quantification of N_2O via headspace gas IR. As a cautionary note, experiments performed under limiting H$^+$ conditions reveal that several competing paths exist that could prevent the release of HNO, one of which involves the formation of the corresponding dinitrosyl {Co(NO)$_2$}^{10} complex **5** as a potential dead end. However, this limitation is somewhat muted by the fact that **5** may also generate HNO. Nitroxyl trapping experiments with Mn^{III}–P and metMb conducted under physiological conditions are consistent with free HNO being released from **3** and **4** with the Co^{II}–HNO intermediate being generated along the reaction path. The enhanced reactivity of **3** and **4** in water is in stark contrast to the relative inertness of {CoNO}^{8} **1** and **2** and can be explained by the increased lability of the Co–NO bond resulting from the *primarily* Co-centered reduction in the {CoNO}^{9} complexes. Numerous {CoNO}^{8} complexes have been synthesized, and the results presented here and elsewhere[43,55,56] suggest that many could be reasonable HNO donors. However, their one-electron reduced {CoNO}^{9} analogues are even more promising, especially as HNO donors in aqueous media. Taken together, this work provides the first example of an extensively characterized set of {CoNO}$^{8/9}$ complexes and suggests that these types of molecules will likely play a role in the development of HNO donors.

In order to apply these complexes for biomedical HNO-release, several properties must still be optimized. For example, the {CoNO}^{8}/{CoNO}^{9} potential is too negative ($E_{1/2}$ ~ −1 V

DOI: 10.1021/jacs.6b05896
J. Am. Chem. Soc. 2016, 138, 12459–12471

vs NHE) to be useful under physiological conditions and the aqueous solubility of the complexes needs to be improved. Based on the similarities in electronic structure and reactivity between **3** and **4**, it is clear that changes to the primary coordination sphere (rather than peripheral ligand modifications) must occur in order to significantly modulate the properties of the M−NO unit. The fine-tuning of these properties can be accomplished by judicious ligand design in future constructs. For example, supporting ligands with neutral donors will: (i) make the corresponding Co−NO complexes charged, and thus more water-soluble in both $\{CoNO\}^8$ and $\{CoNO\}^9$ states; (ii) increase $E_{1/2}$ such that the $\{CoNO\}^9$ state is accessible and stable in the biological window, as this state is the most likely HNO donor; and (iii) increase the lability of the coordinated HNO by decreasing π-backdonation from Co due to reduced charge on the metal. Although dimerization is not observed here, synthetic strategies that encourage HNO liberation and prevent dimerization and subsequent nitroxyl coupling reactions (i.e., NOR reaction) should be considered. Secondary-sphere modifications to protect the Co−NO pocket should accomplish such a goal. Another design component to consider is the use of pentacoordinate supporting ligands to restrict NO chemistry to one specific coordination site and prevent alternative reaction pathways (e.g, dinitrosyl formation). On the other hand, the Co(LN_4)−NO complexes presented here do not show any affinity for a sixth ligand due to the strong trans influence of the NO axial ligand. It appears that Co−NO complexes in biology are rather stable. Indeed, NO has a high affinity for Co^{II}−Cbl ($k_{on} = 5.0 \times 10^8$ M^{-1} s^{-1}; $k_{off} = 3.0$ s^{-1})[132] to generate the $\{CoNO\}^8$, comparable to ferrous-hemes,[133] and labilizes the benzimidazole ligand (Co−$N_{imidazole}$: 2.35 Å).[134] Similar k_{on} values are observed with 5C base-off Cbl and cobinamide (Cbi), but the back reaction is even less favored ($k_{off} = 1.7$ s^{-1} (base-off Cbl);[135] $k_{off} = 0.019$ s^{-1} (Cbi)).[132] Collectively, these design elements are being tested and are the subject of ongoing work in our lab.

EXPERIMENTAL SECTION

General Information. All reagents were purchased from commercial suppliers and used as received unless otherwise noted. Research grade nitric oxide gas (NO(g), UHP, 99.5%) was obtained from Matheson Tri-Gas. The NO(g) was purified by passage through an Ascarite II (sodium hydroxide-coated silica, purchased from Aldrich) column and handled under anaerobic conditions. ^{15}NO(g) ($^{15}N \geq 98\%$) was procured from Cambridge Isotope Laboratories and used as received. 18-crown-6 ether (18C6) was obtained from Aldrich and used as received. Piloty's Acid (PA) was used as received from Cayman Chemical and stored at −20 °C. The Piloty's Acid solution used for the N_2O calibration curve was prepared with milli-Q H_2O and adjusted with NaOH to pH 13.0. Acetonitrile (MeCN), tetrahydrofuran (THF), dichloromethane (CH_2Cl_2), and diethyl ether (Et_2O) were purified by passage through activated alumina columns using an MBraun MB-SPS solvent purification system and stored over 3 Å molecular sieves under an N_2 atmosphere before use. Anhydrous 2-methyltetrahydrofuran (2-MeTHF) and methanol (MeOH) were obtained by storage over 3 Å molecular sieves for 48 h, decanting from the sieves, and storage under N_2. $(Et_4N)_2[CoCl_4]$,[136] LN_4-ligands (N^1E,N^2E)-N^1,N^2-bis((1H-pyrrol-2-yl)methylene)-benzene-1,2-diamine ($LN_4H_2^{Ph}$, where H = dissociable protons), (N^1E,N^2E)-N^1,N^2-bis((1H-pyrrol-2-yl)methylene)-4,5-dichlorobenzene-1,2-diamine ($LN_4H_2^{PhCl}$),[42] $\{CoNO\}^8$ complexes [Co(LN_4^{PhCl})(NO)] (**2**) and [Co(LN_4^{PhCl})(^{15}NO)] (**2-^{15}NO**)[43] were synthesized according to the published procedures. All reactions were performed under an inert atmosphere of N_2 using standard Schlenk-line techniques or in an MBraun Unilab glovebox under an atmosphere of purified N_2. Reactions involving NO(g) and nitroxyl transfer were performed with minimal light exposure by wrapping the reaction flasks/vials with aluminum foil to avoid any photochemical reactions.

Physical Methods. FTIR spectra were collected with a Thermo Nicolet 6700 spectrophotometer running the OMNIC software. Solid-state samples were run as KBr pellets, while solution-state spectra were obtained using a demountable airtight liquid IR cell from Graseby-Specac with CaF_2 windows and 0.1 mm Teflon spacers. All FTIR samples were prepared inside a glovebox under an inert atmosphere of purified N_2. The closed liquid cell was taken out of the box and spectra were acquired immediately. X-band (9.60 GHz) EPR spectra were obtained on a Bruker ESP 300E EPR spectrometer controlled with a Bruker microwave bridge at 10 K. The EPR was equipped with a continuous-flow liquid He cryostat and a temperature controller (ESR 9) made by Oxford Instruments Inc. Continuous wave (CW) Q-band (35 GHz) EPR spectra were recorded at 2 K on a modified Varian spectrometer.[137] Under the experimental conditions employed here, which lead to "rapid-passage" effects,[138] 35 GHz EPR spectra are observed in the dispersion mode and appear as absorption lineshapes, rather than the standard absorption mode detection and first derivative presentation. Digital derivatives were taken to allow conventional presentation. EPR simulations were performed using the program QPOW,[139] as modified by J. Telser. Electronic absorption spectra were run at 298 or 310 K using a Cary-50 UV−vis spectrophotometer containing a Quantum Northwest TC 125 temperature control unit. The UV−vis samples were prepared anaerobically in gastight screw cap quartz cells with an optical pathlength of 1 cm. Electrochemistry measurements were performed with a PAR Model 273A potentiostat using a nonaqueous Ag/Ag^+ (0.01 M $AgNO_3$/0.1 M $^nBu_4NPF_6$ in MeCN) reference electrode, Pt-wire counter electrode, and a Glassy Carbon working milli-electrode (diameter = 2 mm) under an Ar atmosphere. Measurements were performed at ambient temperature using 1.0−10.0 mM analyte in MeCN containing 0.1 M $^nBu_4NPF_6$ as the supporting electrolyte. Ferrocene (Fc) was used as an external standard and all potentials are reported relative to the Fc/Fc^+ couple. ^{1}H, and ^{15}N spectra were recorded in the listed deuterated solvent with a 400 MHz Bruker BZH 400/52 NMR spectrometer or a Varian Unity Inova 500 MHz NMR spectrometer at 298 K or RT with chemical shifts internally referenced to TMS, CH_3NO_2 (^{15}N), or the residual protio signal of the deuterated solvent as previously reported.[140] Low resolution ESI-MS data were collected on a Bruker Esquire 3000 plus ion trap mass spectrometer. High resolution ESI-MS data were collected using an Orbitrap Elite system with CID for MS-MS with precision to the third decimal place. Elemental microanalyses for C, H, and N were performed by ALS Environmental (formerly Columbia Analytical Services) in Tucson, AZ or QTI-Intertek in Whitehouse, NJ.

Computational Methods. DFT calculations were carried out with the ADF (Amsterdam Density Functional) 2013 program,[141] with three different exchange correlation functionals,[142] including the pure functionals BP86[143−145] and OLYP,[146−149] and the hybrid functional B3LYP.[150,151] All-electron STO-TZP basis sets were employed throughout, along with a fine mesh for numerical integration of matrix elements and tight criteria for both SCF and geometry optimizations.

Synthesis of Compounds. *[Co(LN_4^{Ph})(NO)], $\{CoNO\}^8$ (**1**).* To a batch of yellow $LN_4H_2^{Ph}$ (350.0 mg, 1.334 mmol) in 4 mL of MeCN, a 2 mL MeCN slurry of NaH (72.1 mg, 3.00 mmol) was added. A slightly heterogeneous dark yellow solution resulted from mixing the two reactants and H_2 gas was evolved. This solution stirred with quick vacuum for 30 min, following which a 5 mL blue MeCN slurry of $(Et_4N)_2[CoCl_4]$ (615.4 mg, 1.334 mmol) was added. Upon mixing the Co^{II} salt and the deprotonated ligand, the solution immediately turned deep red-brown and a light gray solid slowly precipitated. The reaction mixture stirred at 60 °C with a water bath for 3 h. After cooling the reaction to RT, the solution was filtered to remove NaCl and washed with 3 mL of MeCN. The yellow-tinted dark brown MeCN filtrate containing $(Et_4N)_2[Co(LN_4^{Ph})Cl_2]$ was then purged with purified NO(g) for 1.5 min at 60 °C. Addition of NO resulted in an immediate albeit slight color change; the solution became darker brown (red-tinted) and a microcrystalline precipitate was immediately observed.

DOI: 10.1021/jacs.6b05896
J. Am. Chem. Soc. 2016, 138, 12459−12471

The reaction mixture stirred at 60 °C for 30 min under an NO atmosphere. The solution was then cooled to RT and excess NO(g) was removed by pulling vacuum and refilling with N_2. The reaction mixture was then placed in a −24 °C freezer overnight to induce further precipitation. The resulting microcrystalline solid was filtered, washed (3 × 1 mL) with MeCN and dried under vacuum to afford 391.3 mg (1.120 mmol, 84%) of product. ^{1}H NMR (500 MHz, THF, δ from residual protio solvent): 8.13 (s, 1H), 7.58 (br m, 1H), 7.51 (s, 1H), 7.08 (br m, 1H), 7.00 (s, 1H), 6.33 (s, 1H). ^{13}C NMR (125 MHz, THF-d_8, RT, δ from solvent): 153.0 (*C*H═N), 147.5 (Ar-*C*), 143.9 (Ar-*C*), 142.4 (Ar-*C*), 126.7 (Ar-*C*), 122.2 (Ar-*C*), 116.4 (Ar-*C*), 114.9 (Ar-*C*). FTIR (KBr matrix), ν_{max} (cm^{-1}): 3293 (vw), 3059 (vw), 3010 (vw), 1667 (sh, vs, ν_{NO}), 1656 (vs, ν_{NO}), 1582 (m), 1552 (vs), 1507 (m), 1460 (m), 1446 (m), 1406 (w), 1380 (vs), 1326 (w), 1295 (vs), 1257 (s), 1196 (m), 1170 (w), 1154 (w), 1102 (w), 1076 (w), 1042 (s), 1033 (vs), 986 (m), 929 (w), 914 (w), 895 (m), 863 (w), 846 (w), 816 (w), 781 (w), 741 (vs), 729 (s), 677 (m), 648 (w), 627 (w), 603 (m), 532 (w), 480 (w). FTIR (solution, CaF_2 windows, 0.1 mm spacers, RT), ν_{NO} (cm^{-1}): 1668 (THF), 1670 (MeOH), 1668 (MeCN). UV−vis (THF, 298 K), λ_{max}, nm (ε, M^{-1} cm^{-1}): 318 (19,000), 364 (25,000), 453 (12,000), 497 (9,600). Anal. Calcd for $C_{16}H_{12}CoN_5O\bullet0.5H_2O$: C, 53.64; H, 3.66; N, 19.55. Found: C, 53.75; H, 3.30; N, 19.23.

[Co(LN$_4^{Ph}$)(^{15}NO)], {Co^{15}NO}^{8} ***(1-^{15}NO)***. The isotopically labeled complex **1-^{15}NO** was prepared analogously to **1** except for using 0.2000 g (0.7625 mmol) of $LN_4H_2^{Ph}$, 41.2 mg (1.72 mmol) of NaH, 351.7 g (0.7625 mmol) of $(Et_4N)_2[CoCl_4]$, and ^{15}NO(g). Yield: 0.1421 g (0.4057 mmol, 53%). FTIR (KBr matrix), ν_{NO} (cm^{-1}): 1641 ($\Delta\nu_{NO}$: 26 cm^{-1}), 1628 ($\Delta\nu_{NO}$: 28 cm^{-1}). ^{15}N NMR (50.7 MHz, THF-d_8, δ from CH_3NO_2): 675.

[K(18C6)][Co(LN$_4^{Ph}$)(NO)], {CoNO}^{9} ***(3)***. Solid KC_8 (31.0 mg, 0.229 mmol) was directly added to a 4 mL 2-MeTHF solution of **1** (50.0 mg, 0.143 mmol) containing 18C6 (75.6 mg, 0.286 mmol) and stirred for 1 h at RT. The color of the solution remained dark brown and the color of the insoluble KC_8 slowly changed from gold to silver flakes. The reaction was filtered, yielding insoluble silver flakes (graphite) and a dark brown filtrate, which was then dried *in vacuo* leaving a sticky residue. The sticky residue stirred in ∼15 mL of Et_2O for 2 h in order to remove the excess 18C6 and was then filtered, affording 65.0 mg of **2** as a dark brown solid (0.0996 mmol, 70%). FTIR (KBr matrix), ν_{max} (cm^{-1}): 3078 (w), 2901 (m), 1609 (m, ν_{NO}), 1581 (s), 1557 (s), 1457 (m), 1382 (s), 1351 (m), 1285 (s), 1253 (m), 1213 (w), 1187 (m), 1105 (vs), 1025 (m), 961 (m), 920 (w), 867 (w), 836 (w), 784 (w), 759 (w), 736 (m), 687 (w), 610 (w), 592 (w), 583 (w), 525 (w), 477 (w), 450 (w), 419 (w). HRMS-ESI (m/z): [M]$^-$ calcd for $C_{16}H_{12}CoN_5O_1$ (relative abundance), 349.037 (100.0), 350.040 (17.3), 351.043 (1.2); found, 349.037 (100.0), 350.040 (14.4), 351.029 (0.8). UV−vis (THF, 298 K), λ_{max}, nm (ε, M^{-1} cm^{-1}): 317 (5,900), 365 (9,600), 451 (3,700), 498 (2,400). Anal. Calcd for $C_{28}H_{36}CoKN_5O_7$: C, 51.53; H, 5.56; N, 10.73. Found: C, 51.05; H, 5.69; N, 10.21.

[K(18C6)][Co(LN$_4^{Ph}$)(^{15}NO)], {Co^{15}NO}^{9} ***(3-^{15}NO)***. The isotopically labeled complex **3-^{15}NO** was prepared analogously to **3** except for using 50.0 mg (0.143 mmol) of **1-^{15}NO**, 30.9 mg (0.229 mmol) of KC_8, and 75.5 mg (0.286 mmol) of 18C6. Yield: 68.7 mg (0.105 mmol, 74% yield). FTIR (KBr matrix), ν_{NO} (cm^{-1}): ∼ 1580; overlaps with broad imine stretches ($\nu_{C=N}$) in the same region. HRMS-ESI (m/z): [M]$^-$ calcd for $C_{16}H_{12}CoN_4{}^{15}N_1O_1$ (relative abundance), 350.034 (100.0), 351.037 (17.3), 352.040 (1.4); found, 350.035 (100.0), 351.038 (17.3), 352.037 (1.2).

[K(18C6)][Co(LN$_4^{PhCl}$)(NO)], {CoNO}^{9} ***(4)***. Solid KC_8 (25.9 mg, 0.191 mmol) was directly added to a 4 mL 2-MeTHF solution of **2** (50.0 mg, 0.120 mmol) containing 18C6 (63.2 mg, 0.239 mmol) and stirred for 1 h at RT. The color of the solution remained dark brown and the KC_8 slowly changed from gold to silver consistent with formation of graphite. The reaction mixture was filtered with a medium porosity glass frit to remove the insoluble silver graphite flakes. The resulting dark brown filtrate was then stripped to dryness in vacuo leaving a sticky residue. This residue was stirred in ∼10 mL of Et_2O for 20 min in order to remove the excess 18C6, which afforded 70.4 mg (0.0976 mmol, 82%) of a dark brown solid after vacuum filtration and drying. FTIR (KBr matrix), ν_{max} (cm^{-1}): 3092 (w), 3079 (w), 2908 (m), 2892 (m), 2855 (m), 2823 (w), 2797 (w), 1617 (m, ν_{NO}), 1568 (vs), 1537 (s), 1455 (m), 1380 (s), 1350 (m), 1292 (s), 1270 (m), 1249 (w), 1191 (w), 1110 (vs), 1026 (m), 963 (m), 932 (w), 889 (w), 866 (w), 838 (w), 808 (w), 760 (w), 741 (w), 685 (w), 673 (w), 608 (w), 531 (w), 494 (w), 467 (w), 450 (w), 432 (w) 417 (w), 405 (w). HRMS-ESI (m/z): [M]$^-$ calcd for $C_{16}H_{10}Cl_2CoN_5O_1$ (relative abundance), 416.959 (100.0), 417.963 (17.3), 418.956 (64.8), 419.959 (11.2), 420.953 (10.5), 421.957 (1.8); found, 416.960 (100.0), 417.980 (23.5), 418.957 (65.9), 419.977 (15.0), 420.954 (10.0), 421.973 (1.9). UV−vis (THF, 298 K), λ_{max}, nm (ε, M^{-1} cm^{-1}): 324 (5,000), 370 (8,400), 460 (3,700), 510 (2,300). Anal. Calcd for $C_{28}H_{34}Cl_2CoKN_5O_7\bullet H_2O$: C, 45.47; H, 4.91; N, 9.47. Found: C, 45.40; H, 4.45; N, 9.27.

[K(18C6)][Co(LN$_4^{PhCl}$)(^{15}NO)], {Co^{15}NO}^{9} ***(4-^{15}NO)***. The isotopically labeled complex **4-^{15}NO** was prepared analogously to **4** except for using 50.1 mg (0.120 mmol) of **2-^{15}NO**, 25.9 mg (0.192 mmol) of KC_8, and 63.2 mg (0.239 mmol) of 18C6. Yield: 57.0 mg (0.0789 mmol, 66% yield). FTIR (KBr matrix), ν_{NO} (cm^{-1}): ∼ 1585, unable to definitively identify ν_{15NO} due to broad imine stretches ($\nu_{C=N}$) in the same region. HRMS-ESI (m/z): [M]$^-$ calcd for $C_{16}H_{10}Cl_2CoN_4{}^{15}N_1O_1$ (relative abundance), 417.956 (100.0), 418.959 (17.3), 419.953 (63.9), 420.956 (11.1), 421.950 (10.2), 422.953 (1.8); found, 417.958 (100.0), 418.960 (17.8), 419.954 (67.8), 420.957 (11.3), 421.951 (10.9), 422.954 (1.7).

■ ASSOCIATED CONTENT

Ⓢ Supporting Information

The Supporting Information is available free of charge on the ACS Publications website at DOI: 10.1021/jacs.6b05896.

Additional reactivity, structural, and spectroscopic data (PDF)

CIF file for **1** (CIF)

■ AUTHOR INFORMATION

Corresponding Author

*tharrop@uga.edu

Notes

The authors declare no competing financial interest.

■ ACKNOWLEDGMENTS

T.C.H. acknowledges financial support from the NSF, the Office of the Vice President for Research (OVPR), and the Office of the Provost at the University of Georgia (UGA). The authors also acknowledge the work of Koustubh S. Dube (UGA) for the initial synthesis of **1**. T.L.S. and S.P.D. acknowledge the NIH and the American Heart Association/Friedreich's Ataxia Research Alliance (DK068139 (T.L.S.), DK101230 and 14PRE18830036 (S.P.D.)) for research funding. We thank Dennis R. Phillips and Chau-Wen Chou from the Proteomics and Mass Spectrometry Core Facility (PAMS) at UGA for their assistance with MS experiments. PAMS Instrumentation was purchased in part with funds from NIH Grant 1S10RR028859-01. Funds for PAMS facility operations were provided by the UGA OVPR and the UGA Department of Chemistry. We thank Brian M. Hoffman, Northwestern University, for use of the X- and Q-band EPR spectrometers, which is supported by the NIH (GM 111097 to B.M.H.). XAS studies were performed at the Stanford Synchrotron Radiation Lightsource (SSRL) and at the National Synchrotron Radiation Laboratory (NSLS) on beamline X3b. SSRL is a national user facility operated by Stanford University on behalf of the Department of Energy (DOE), Office of Basic

DOI: 10.1021/jacs.6b05896
J. Am. Chem. Soc. 2016, 138, 12459−12471

Energy Sciences. The SSRL Structural Molecular Biology Program is supported by the DOE, Office of Biological and Environmental Research, and by the NIH, National Center for Research Resources, Biomedical Technology Program. NSLS, located at Brookhaven National Laboratory, is supported by the DOE, Division of Materials Sciences and Division of Chemical Sciences, under Contract No. DEAC02-98CH10886.

REFERENCES

(1) Bartberger, M. D.; Liu, W.; Ford, E.; Miranda, K. M.; Switzer, C.; Fukuto, J. M.; Farmer, P. J.; Wink, D. A.; Houk, K. N. *Proc. Natl. Acad. Sci. U. S. A.* **2002**, *99*, 10958.
(2) Speelman, A. L.; Lehnert, N. *Acc. Chem. Res.* **2014**, *47*, 1106.
(3) Kumar, M. R.; Fukuto, J. M.; Miranda, K. M.; Farmer, P. J. *Inorg. Chem.* **2010**, *49*, 6283.
(4) Lehnert, N.; Scheidt, W. R.; Wolf, M. W. *Struct. Bonding (Berlin, Ger.)* **2013**, *154*, 155.
(5) Shiro, Y.; Fujii, M.; Iizuka, T.; Adachi, S.-i.; Tsukamoto, K.; Nakahara, K.; Shoun, H. *J. Biol. Chem.* **1995**, *270*, 1617.
(6) Daiber, A.; Nauser, T.; Takaya, N.; Kudo, T.; Weber, P.; Hultschig, C.; Shoun, H.; Ullrich, V. *J. Inorg. Biochem.* **2002**, *88*, 343.
(7) Obayashi, E.; Takahashi, S.; Shiro, Y. *J. Am. Chem. Soc.* **1998**, *120*, 12964.
(8) Zheng, S.; Berto, T. C.; Dahl, E. W.; Hoffman, M. B.; Speelman, A. L.; Lehnert, N. *J. Am. Chem. Soc.* **2013**, *135*, 4902.
(9) Maia, L. B.; Moura, J. J. G. *Chem. Rev.* **2014**, *114*, 5273.
(10) Bykov, D.; Neese, F. *Inorg. Chem.* **2015**, *54*, 9303.
(11) Enemark, J. H.; Feltham, R. D. *Coord. Chem. Rev.* **1974**, *13*, 339. $\{MNO\}^n$, where n = number of metal d + NO π^* electrons.
(12) Lin, R.; Farmer, P. J. *J. Am. Chem. Soc.* **2000**, *122*, 2393.
(13) Sulc, F.; Immoos, C. E.; Pervitsky, D.; Farmer, P. J. *J. Am. Chem. Soc.* **2004**, *126*, 1096.
(14) Brown, K. L. *Chem. Rev.* **2005**, *105*, 2075.
(15) Pallares, I. G.; Brunold, T. C. *Inorg. Chem.* **2014**, *53*, 7676.
(16) Brouwer, M.; Chamulitrat, W.; Ferruzzi, G.; Sauls, D. L.; Weinberg, J. B. *Blood* **1996**, *88*, 1857.
(17) Subedi, H.; Hassanin, H. A.; Brasch, N. E. *Inorg. Chem.* **2014**, *53*, 1570.
(18) Subedi, H.; Brasch, N. E. *Eur. J. Inorg. Chem.* **2015**, *2015*, 3825.
(19) Subedi, H.; Brasch, N. E. *Dalton Trans.* **2016**, *45*, 352.
(20) Carmel, R.; Jacobsen, D. W. *Homocysteine in Health and Disease*; Cambridge University Press: Cambridge, U.K., 2001.
(21) Qureshi, G. A.; Memon, S. A.; Collin, C.; Parvez, S. H. *Biog. Amines* **2003**, *18*, 117.
(22) Fukuto, J. M.; Carrington, S. J. *Antioxid. Redox Signaling* **2011**, *14*, 1649.
(23) Paolocci, N.; Jackson, M. I.; Lopez, B. E.; Miranda, K.; Tocchetti, C. G.; Wink, D. A.; Hobbs, A. J.; Fukuto, J. M. *Pharmacol. Ther.* **2007**, *113*, 442.
(24) Flores-Santana, W.; Salmon, D. J.; Donzelli, S.; Switzer, C. H.; Basudhar, D.; Ridnour, L.; Cheng, R.; Glynn, S. A.; Paolocci, N.; Fukuto, J. M.; Miranda, K. M.; Wink, D. A. *Antioxid. Redox Signaling* **2011**, *14*, 1659.
(25) Moncada, S.; Higgs, E. A. *Br. J. Pharmacol.* **2006**, *147*, S193.
(26) Irvine, J. C.; Ritchie, R. H.; Favaloro, J. L.; Andrews, K. L.; Widdop, R. E.; Kemp-Harper, B. K. *Trends Pharmacol. Sci.* **2008**, *29*, 601.
(27) Paolocci, N.; Saavedra, W. F.; Miranda, K. M.; Martignani, C.; Isoda, T.; Hare, J. M.; Espey, M. G.; Fukuto, J. M.; Feelisch, M.; Wink, D. A.; Kass, D. A. *Proc. Natl. Acad. Sci. U. S. A.* **2001**, *98*, 10463.
(28) Rosen, G. M.; Tsai, P.; Pou, S. *Chem. Rev.* **2002**, *102*, 1191.
(29) Eberhardt, M.; Dux, M.; Namer, B.; Miljkovic, J.; Cordasic, N.; Will, C.; Kichko, T. I.; de la Roche, J.; Fischer, M.; Suárez, S. A.; Bikiel, D.; Dorsch, K.; Leffler, A.; Babes, A.; Lampert, A.; Lennerz, J. K.; Jacobi, J.; Martí, M. A.; Doctorovich, F.; Högestätt, E. D.; Zygmunt, P. M.; Ivanovic-Burmazovic, I.; Messlinger, K.; Reeh, P.; Filipovic, M. R. *Nat. Commun.* **2014**, *5*, 4381.
(30) Miljkovic, J. L.; Kenkel, I.; Ivanović-Burmazović, I.; Filipovic, M. R. *Angew. Chem., Int. Ed.* **2013**, *52*, 12061.
(31) Filipovic, M. R.; Eberhardt, M.; Prokopovic, V.; Mijuskovic, A.; Orescanin-Dusic, Z.; Reeh, P.; Ivanović-Burmazović, I. *J. Med. Chem.* **2013**, *56*, 1499.
(32) Wedmann, R.; Zahl, A.; Shubina, T. E.; Dürr, M.; Heinemann, F. W.; Bugenhagen, B. E. C.; Burger, P.; Ivanović-Burmazović, I.; Filipovic, M. R. *Inorg. Chem.* **2015**, *54*, 9367.
(33) Suarez, S. A.; Neuman, N. I.; Muñoz, M.; Álvarez, L.; Bikiel, D. E.; Brondino, C. D.; Ivanović-Burmazović, I.; Miljkovic, J. L.; Filipovic, M. R.; Martí, M. A.; Doctorovich, F. *J. Am. Chem. Soc.* **2015**, *137*, 4720.
(34) Shafirovich, V.; Lymar, S. V. *Proc. Natl. Acad. Sci. U. S. A.* **2002**, *99*, 7340.
(35) Miranda, K. M. *Coord. Chem. Rev.* **2005**, *249*, 433.
(36) Kohout, F. C.; Lampe, F. W. *J. Am. Chem. Soc.* **1965**, *87*, 5795.
(37) Smith, P. A. S.; Hein, G. E. *J. Am. Chem. Soc.* **1960**, *82*, 5731.
(38) Angeli, A.; Angelico, F.; Scurti, F. *Chem. Zentralbl.* **1902**, *73*, 691.
(39) DeMaster, E. G.; Redfern, B.; Nagasawa, H. T. *Biochem. Pharmacol.* **1998**, *55*, 2007.
(40) Nagasawa, H. T.; DeMaster, E. G.; Redfern, B.; Shirota, F. N.; Goon, D. J. W. *J. Med. Chem.* **1990**, *33*, 3120.
(41) Patra, A. K.; Dube, K. S.; Sanders, B. C.; Papaefthymiou, G. C.; Conradie, J.; Ghosh, A.; Harrop, T. C. *Chem. Sci.* **2012**, *3*, 364.
(42) Sanders, B. C.; Patra, A. K.; Harrop, T. C. *J. Inorg. Biochem.* **2013**, *118*, 115.
(43) Rhine, M. A.; Rodrigues, A. V.; Bieber Urbauer, R. J.; Urbauer, J. L.; Stemmler, T. L.; Harrop, T. C. *J. Am. Chem. Soc.* **2014**, *136*, 12560.
(44) McCleverty, J. A. *Chem. Rev.* **2004**, *104*, 403 and references therein.
(45) Wyllie, G. R. A.; Scheidt, W. R. *Chem. Rev.* **2002**, *102*, 1067 and references therein.
(46) Wright, A. M.; Hayton, T. W. *Comments Inorg. Chem.* **2012**, *33*, 207 and references therein.
(47) Ellison, M. K.; Scheidt, W. R. *Inorg. Chem.* **1998**, *37*, 382.
(48) Fujita, E.; Chang, C. K.; Fajer, J. *J. Am. Chem. Soc.* **1985**, *107*, 7665.
(49) Franz, K. J.; Doerrer, L. H.; Spingler, B.; Lippard, S. J. *Inorg. Chem.* **2001**, *40*, 3774.
(50) Kozhukh, J.; Lippard, S. J. *J. Am. Chem. Soc.* **2012**, *134*, 11120.
(51) Hess, J. L.; Conder, H. L.; Green, K. N.; Darensbourg, M. Y. *Inorg. Chem.* **2008**, *47*, 2056.
(52) Uyeda, C.; Peters, J. C. *J. Am. Chem. Soc.* **2013**, *135*, 12023.
(53) Kumar, P.; Lee, Y.-M.; Hu, L.; Chen, J.; Park, Y. J.; Yao, J.; Chen, H.; Karlin, K. D.; Nam, W. *J. Am. Chem. Soc.* **2016**, *138*, 7753.
(54) Kumar, P.; Lee, Y.-M.; Park, Y. J.; Siegler, M. A.; Karlin, K. D.; Nam, W. *J. Am. Chem. Soc.* **2015**, *137*, 4284.
(55) Doyle, M. P.; Pickering, R. A.; Dykstra, R. L.; Cook, B. R. *J. Am. Chem. Soc.* **1982**, *104*, 3392. The species responsible for release of the NO moiety may be a reduced cobalt nitrosyl, given the presence of excess reductant.
(56) Doyle, M. P.; Van Doornik, F. J.; Funckes, C. L. *Inorg. Chim. Acta* **1980**, *46*, L111. $[Co(NH_3)_5(NO)]Cl_2$ reacts with both Fe^{III}- and Fe^{II}-heme proteins.
(57) Ungermann, C. B.; Caulton, K. G. *J. Am. Chem. Soc.* **1976**, *98*, 3862.
(58) Caulton, K. G. *J. Am. Chem. Soc.* **1973**, *95*, 4076.
(59) Blanchard, A. A.; Rafter, J. R.; Adams, W. B., Jr. *J. Am. Chem. Soc.* **1934**, *56*, 16.
(60) Coleman, G. W.; Blanchard, A. A. *J. Am. Chem. Soc.* **1936**, *58*, 2160.
(61) Thyagarajan, S.; Incarvito, C. D.; Rheingold, A. L.; Theopold, K. H. *Inorg. Chim. Acta* **2003**, *345*, 333.
(62) Tomson, N. C.; Crimmin, M. R.; Petrenko, T.; Rosebrugh, L. E.; Sproules, S.; Boyd, W. C.; Bergman, R. G.; DeBeer, S.; Toste, F. D.; Wieghardt, K. *J. Am. Chem. Soc.* **2011**, *133*, 18785.
(63) Sacconi, L.; Ghilardi, C. A.; Mealli, C.; Zanobini, F. *Inorg. Chem.* **1975**, *14*, 1380.

DOI: 10.1021/jacs.6b05896
J. Am. Chem. Soc. 2016, 138, 12459−12471

(64) Di Vaira, M.; Ghilardi, C. A.; Sacconi, L. *Inorg. Chem.* **1976**, *15*, 1555.
(65) Chuang, C.-H.; Liaw, W.-F.; Hung, C.-H. *Angew. Chem., Int. Ed.* **2016**, *55*, 5190.
(66) Broderick, K. E.; Alvarez, L.; Balasubramanian, M.; Belke, D. D.; Makino, A.; Chan, A.; Woods, V. L., Jr.; Dillmann, W. H.; Sharma, V. S.; Pilz, R. B.; Bigby, T. D.; Boss, G. R. *Exp. Biol. Med.* **2007**, *232*, 1432. The species responsible for release of the NO moiety may be a reduced cobalt nitrosyl, given the presence of excess reductant.
(67) McCrory, C. C. L.; Uyeda, C.; Peters, J. C. *J. Am. Chem. Soc.* **2012**, *134*, 3164.
(68) Stubbert, B. D.; Peters, J. C.; Gray, H. B. *J. Am. Chem. Soc.* **2011**, *133*, 18070.
(69) Valdez, C. N.; Dempsey, J. L.; Brunschwig, B. S.; Winkler, J. R.; Gray, H. B. *Proc. Natl. Acad. Sci. U. S. A.* **2012**, *109*, 15589.
(70) Zee, D. Z.; Chantarojsiri, T.; Long, J. R.; Chang, C. J. *Acc. Chem. Res.* **2015**, *48*, 2027 and references therein.
(71) Kelley, P.; Day, M. W.; Agapie, T. *Eur. J. Inorg. Chem.* **2013**, *2013*, 3840.
(72) Basu, D.; Mazumder, S.; Niklas, J.; Baydoun, H.; Wanniarachchi, D.; Shi, X.; Staples, R. J.; Poluektov, O.; Schlegel, H. B.; Verani, C. N. *Chem. Sci.* **2016**, *7*, 3264.
(73) Ding, K.; Brennessel, W. W.; Holland, P. L. *J. Am. Chem. Soc.* **2009**, *131*, 10804.
(74) Betley, T. A.; Peters, J. C. *J. Am. Chem. Soc.* **2003**, *125*, 10782.
(75) Chapovetsky, A.; Do, T. H.; Haiges, R.; Takase, M. K.; Marinescu, S. C. *J. Am. Chem. Soc.* **2016**, *138*, 5765.
(76) Mason, J.; Larkworthy, L. F.; Moore, E. A. *Chem. Rev.* **2002**, *102*, 913.
(77) Addison, A. W.; Rao, T. N.; Reedijk, J.; van Rijn, J.; Verschoor, G. C. *J. Chem. Soc., Dalton Trans.* **1984**, 1349.
(78) Pellegrino, J.; Bari, S. E.; Bikiel, D. E.; Doctorovich, F. *J. Am. Chem. Soc.* **2010**, *132*, 989.
(79) Sanders, B. C.; Rhine, M. A.; Harrop, T. C. *Struct. Bonding (Berlin, Ger.)* **2013**, *160*, 57.
(80) Harrop, T. C. *Adv. Inorg. Chem.* **2015**, *67*, 243.
(81) Gautam, R.; Loughrey, J. J.; Astashkin, A. V.; Shearer, J.; Tomat, E. *Angew. Chem., Int. Ed.* **2015**, *54*, 14894.
(82) Ramdhanie, B.; Telser, J.; Caneschi, A.; Zakharov, L. N.; Rheingold, A. L.; Goldberg, D. P. *J. Am. Chem. Soc.* **2004**, *126*, 2515.
(83) Fujii, H.; Dou, Y.; Zhou, H.; Yoshida, T.; Ikeda-Saito, M. *J. Am. Chem. Soc.* **1998**, *120*, 8251.
(84) Little, R. G.; Hoffman, B. M.; Ibers, J. A. *Bioinorg. Chem.* **1974**, *3*, 207.
(85) Wayland, B. B.; Minkiewicz, J. V.; Abd-Elmageed, M. E. *J. Am. Chem. Soc.* **1974**, *96*, 2795.
(86) Wayland, B. B.; Abd-Elmageed, M. E. *J. Am. Chem. Soc.* **1974**, *96*, 4809.
(87) McGarvey, B. R. *Can. J. Chem.* **1975**, *53*, 2498.
(88) Solomon, E. I.; Heppner, D. E.; Johnston, E. M.; Ginsbach, J. W.; Cirera, J.; Qayyum, M.; Kieber-Emmons, M. T.; Kjaergaard, C. H.; Hadt, R. G.; Tian, L. *Chem. Rev.* **2014**, *114*, 3659.
(89) Garribba, E.; Micera, G. *J. Chem. Educ.* **2006**, *83*, 1229.
(90) Serres, R. G.; Grapperhaus, C. A.; Bothe, E.; Bill, E.; Weyhermüller, T.; Neese, F.; Wieghardt, K. *J. Am. Chem. Soc.* **2004**, *126*, 5138.
(91) Brown, T. G.; Hoffman, B. M. *Mol. Phys.* **1980**, *39*, 1073.
(92) Hori, H.; Ikeda-Saito, M.; Froncisz, W.; Yonetani, T. *J. Biol. Chem.* **1983**, *258*, 12368.
(93) Hyde, J. S.; Froncisz, W. *Annu. Rev. Biophys. Bioeng.* **1982**, *11*, 391.
(94) Liptak, M. D.; Fleischhacker, A. S.; Matthews, R. G.; Telser, J.; Brunold, T. C. *J. Phys. Chem. B* **2009**, *113*, 5245.
(95) Bencze, K. Z.; Kondapalli, K. C.; Stemmler, T. L., X-ray Absorption Spectroscopy. In *Applications of Physical Methods to Inorganic and Bioinorganic Chemistry*; Scott, R. A., Lukehart, C. M., Eds.; John Wiley & Sons, Ltd.: Chichester, UK, 2008; pp 513.
(96) Padden, K. M.; Krebs, J. F.; MacBeth, C. E.; Scarrow, R. C.; Borovik, A. S. *J. Am. Chem. Soc.* **2001**, *123*, 1072.
(97) Wirt, M. D.; Sagi, I.; Chen, E.; Frisbie, S. M.; Lee, R.; Chance, M. R. *J. Am. Chem. Soc.* **1991**, *113*, 5299.
(98) Padden, K. M.; Krebs, J. F.; Trafford, K. T.; Yap, G. P. A.; Rheingold, A. H.; Borovik, A. S.; Scarrow, R. C. *Chem. Mater.* **2001**, *13*, 4305.
(99) Adrait, A.; Jacquamet, L.; Le Pape, L.; Gonzalez de Peredo, A.; Aberdam, D.; Hazemann, J.-L.; Latour, J.-M.; Michaud-Soret, I. *Biochemistry* **1999**, *38*, 6248.
(100) Kleifeld, O.; Rulíšek, L.; Bogin, O.; Frenkel, A.; Havlas, Z.; Burstein, Y.; Sagi, I. *Biochemistry* **2004**, *43*, 7151.
(101) Broad surveys of quantum chemical studies on nitrosyls: (a) Ghosh, A. *Acc. Chem. Res.* **2005**, *38*, 943. (b) Ghosh, A.; Hopmann, K. H.; Conradie, J. In *Computational Inorganic and Bioinorganic Chemistry*; Solomon, E. I., Scott, R. A., King, R. B., Eds.; John Wiley & Sons Ltd: Chichester, UK, 2009; pp 389− 410. (c) Goodrich, L. E.; Paulat, F.; Praneeth, V. K. K.; Lehnert, N. *Inorg. Chem.* **2010**, *49*, 6293. (d) Vazquez-Lima, H.; Conradie, J.; Ghosh, A. *Inorg. Chem.* **2016**, *55*, 8248.
(102) DFT calculations on CoNO complexes: (a) Jaworska, M. *Chem. Phys.* **2007**, *332*, 203. (b) Hopmann, K. H.; Conradie, J.; Tangen, E.; Tonzetich, Z. J.; Lippard, S. J.; Ghosh, A. *Inorg. Chem.* **2015**, *54*, 7362.
(103) The notation A′ 61‖60 means that there are 61 α or spin-up electrons and 60 β or spin-down electrons in the irreducible representation A′ (C_s point group symmetry).
(104) The $\{CoNO\}^9$ porphyrin in ref 65 functions as an NO reductase model and liberates N_2O in THF mixtures with a protic solvent (H_2O, MeOH, EtOH) via a putative N_2O_2-bridged intermediate. For DFT calculations on a $\{CoNO\}^9$ porphyrin, see: Conradie, J.; Ghosh, A. *J. Phys. Chem. B* **2016**, *120*, 4972.
(105) Heinecke, J. L.; Khin, C.; Pereira, J. C. M.; Suárez, S. A.; Iretskii, A. V.; Doctorovich, F.; Ford, P. C. *J. Am. Chem. Soc.* **2013**, *135*, 4007.
(106) Łapiński, A.; Spanget-Larsen, J.; Waluk, J.; Radziszewski, J. G. *J. Chem. Phys.* **2001**, *115*, 1757.
(107) Hughes, M. N.; Cammack, R. *Methods Enzymol.* **1999**, *301*, 279.
(108) $[Co^{III}(LN_4^{Ph})]^+$ and $[Co^{I}(LN_4^{Ph})]^-$ may be the products of $[Co^{II}(LN_4^{Ph})]$ disproportionation.
(109) Reactions of **1** and **2** with $HBF_4{\cdot}Et_2O$ (1:1.3) in THF reveal the presence of trace N_2O by IR.
(110) Tseng, Y.-T.; Chen, C.-H.; Lin, J.-Y.; Li, B.-H.; Lu, Y.-H.; Lin, C.-H.; Chen, H.-T.; Weng, T.-C.; Sokaras, D.; Chen, H.-Y.; Soo, Y.-L.; Lu, T.-T. *Chem. - Eur. J.* **2015**, *21*, 17570.
(111) Chiang, C.-Y.; Darensbourg, M. Y. *J. Biol. Inorg. Chem.* **2006**, *11*, 359.
(112) Goodrich, L. E.; Roy, S.; Alp, E. E.; Zhao, J.; Hu, M. Y.; Lehnert, N. *Inorg. Chem.* **2013**, *52*, 7766.
(113) Reisz, J. A.; Klorig, E. B.; Wright, M. W.; King, S. B. *Org. Lett.* **2009**, *11*, 2719.
(114) Abucayon, E. G.; Khade, R. L.; Powell, D. R.; Zhang, Y.; Richter-Addo, G. B. *J. Am. Chem. Soc.* **2016**, *138*, 104.
(115) Hu, B.; Li, J. *Angew. Chem., Int. Ed.* **2015**, *54*, 10579.
(116) Kupper, C.; Rees, J. A.; Dechert, S.; DeBeer, S.; Meyer, F. *J. Am. Chem. Soc.* **2016**, *138*, 7888.
(117) Martí, M. A.; Bari, S. E.; Estrin, D. A.; Doctorovich, F. *J. Am. Chem. Soc.* **2005**, *127*, 4680.
(118) Álvarez, L.; Suarez, S. A.; Bikiel, D. E.; Reboucas, J. S.; Batinić-Haberle, I.; Martí, M. A.; Doctorovich, F. *Inorg. Chem.* **2014**, *53*, 7351.
(119) Doctorovich, F.; Bikiel, D. E.; Pellegrino, J.; Suárez, S. A.; Martí, M. A. *Acc. Chem. Res.* **2014**, *47*, 2907.
(120) Pereira, J. C. M.; Iretskii, A. V.; Han, R.-M.; Ford, P. C. *J. Am. Chem. Soc.* **2015**, *137*, 328.
(121) Fitzpatrick, J.; Kim, E. *Acc. Chem. Res.* **2015**, *48*, 2453.
(122) Tran, C. T.; Kim, E. *Inorg. Chem.* **2012**, *51*, 10086.
(123) Romberg, R. W.; Kassner, R. J. *Biochemistry* **1979**, *18*, 5387.
(124) Antonini, E.; Brunori, M. *Hemoglobin and Myoglobin in their Reactions with Ligands*; North-Holland Publishing Company: Amsterdam, 1971.

DOI: 10.1021/jacs.6b05896
J. Am. Chem. Soc. 2016, 138, 12459−12471

(125) Andrei, D.; Salmon, D. J.; Donzelli, S.; Wahab, A.; Klose, J. R.; Citro, M. L.; Saavedra, J. E.; Wink, D. A.; Miranda, K. M.; Keefer, L. K. *J. Am. Chem. Soc.* **2010**, *132*, 16526.
(126) The calculated quantitative yield (99%) of MbNO may be high because of light-scattering from insoluble complex or denatured protein, and/or contributing absorbance from the CoNO complex. The latter is more likely, as relatively low concentrations of CoNO complex were used and no precipitation was observed. Second, addition of the same volume of organic solvent to the metMb solution did not change its UV−vis spectrum, thus eliminating any denaturation.
(127) Bazylinski, D. A.; Hollocher, T. C. *J. Am. Chem. Soc.* **1985**, *107*, 7982.
(128) Choi, I.-K.; Liu, Y.; Feng, D.; Paeng, K.-J.; Ryan, M. D. *Inorg. Chem.* **1991**, *30*, 1832.
(129) Gao, Y.; Toubaei, A.; Kong, X.; Wu, G. *Angew. Chem., Int. Ed.* **2014**, *53*, 11547.
(130) Lehnert, N.; Praneeth, V. K. K.; Paulat, F. *J. Comput. Chem.* **2006**, *27*, 1338.
(131) A similar trend has been observed upon protonation of a 6C $\{FeNO\}^8$ complex with ∼0.05 Å increases in Fe−N(O) and N−O. However, there is no spin-state change. See ref 130.
(132) Sharma, V. S.; Pilz, R. B.; Boss, G. R.; Magde, D. *Biochemistry* **2003**, *42*, 8900.
(133) Ford, P. C.; Lorkovic, I. M. *Chem. Rev.* **2002**, *102*, 993.
(134) Hassanin, H. A.; El-Shahat, M. F.; DeBeer, S.; Smith, C. A.; Brasch, N. E. *Dalton Trans.* **2010**, *39*, 10626.
(135) Wolak, M.; Zahl, A.; Schneppensieper, T.; Stochel, G.; van Eldik, R. *J. Am. Chem. Soc.* **2001**, *123*, 9780.
(136) Gill, N. S.; Taylor, F. B. *Inorg. Synth.* **1967**, *9*, 136.
(137) Werst, M. M.; Davoust, C. E.; Hoffman, B. M. *J. Am. Chem. Soc.* **1991**, *113*, 1533.
(138) Mailer, C.; Taylor, C. P. S. *Biochim. Biophys. Acta, Protein Struct.* **1973**, *322*, 195.
(139) Belford, R. L.; Nilges, M. J. In *EPR Symposium, 21st Rocky Mountain Conference*, Denver, CO, August, 1979.
(140) Fulmer, G. R.; Miller, A. J. M.; Sherden, N. H.; Gottlieb, H. E.; Nudelman, A.; Stoltz, B. M.; Bercaw, J. E.; Goldberg, K. I. *Organometallics* **2010**, *29*, 2176.
(141) Te Velde, G.; Bickelhaupt, F. M.; Baerends, E. J.; Fenseca Guerra, C.; Van Gisbergen, S. J. A.; Snijders, J. G.; Ziegler, T. *J. Comput. Chem.* **2001**, *22*, 931.
(142) For a comparison of different exchange-correlation functionals for transition metal systems, see, e.g.: (a) Reiher, M.; Salomon, O.; Hess, B. A. *Theor. Chem. Acc.* **2001**, *107*, 48. (b) Ghosh, A.; Taylor, P. R. *Curr. Opin. Chem. Biol.* **2003**, *7*, 113. (c) Conradie, J.; Swarts, J. C.; Ghosh, A. *J. Phys. Chem. B* **2004**, *108*, 452. (d) Swart, M.; Ehlers, A. W.; Lammertsma, K. *Mol. Phys.* **2004**, *102*, 2467. (e) Conradie, J.; Ghosh, A. *J. Phys. Chem. B* **2007**, *111*, 12621. (f) Hopmann, K. H.; Conradie, J.; Ghosh, A. *J. Phys. Chem. B* **2009**, *113*, 10540. (g) Conradie, M. M.; Conradie, J.; Ghosh, A. *J. Inorg. Biochem.* **2011**, *105*, 84.
(143) Becke, A. D. *Phys. Rev. A: At., Mol., Opt. Phys.* **1988**, *38*, 3098.
(144) Perdew, J. P. *Phys. Rev. B: Condens. Matter Mater. Phys.* **1986**, *33*, 8822.
(145) Erratum: Perdew, J. P. *Phys. Rev. B: Condens. Matter Mater. Phys.* **1986**, *34*, 7406.
(146) Handy, N. C.; Cohen, A. J. *Mol. Phys.* **2001**, *99*, 403.
(147) Lee, C. H.; Yang, W.; Parr, R. G. *Phys. Rev. B: Condens. Matter Mater. Phys.* **1988**, *37*, 785.
(148) Johnson, B. G.; Gill, P. M. W.; Pople, J. A. *J. Chem. Phys.* **1993**, *98*, 5612.
(149) Russo, T. V.; Martin, R. L.; Hay, P. J. *J. Chem. Phys.* **1994**, *101*, 7729.
(150) Becke, A. D. *J. Chem. Phys.* **1993**, *98*, 5648.
(151) Stephens, P. J.; Devlin, F. J.; Chabalowski, C. F.; Frisch, M. J. *J. Phys. Chem.* **1994**, *98*, 11623.

DOI: 10.1021/jacs.6b05896
J. Am. Chem. Soc. 2016, 138, 12459−12471